Universitatea POLITEHNICA din Bucureşti
ŞCOALA DOCTORALĂ DE INGINERIE ELECTRICĂ

DOCTORAL THESIS

- summary -

Contributions to optimizing wireless power transfer for an independent charging base

PhD supervisor:

Prof. Univ. Ph.D. Eng. Mihai Octavian POPESCU

PhD Student:

Eng. Vlad MOCANU

BUCUREŞTI

2023

CONTENTS

1. INTRODUCTION

1.1 Historical development of electromagnetic study

The electromagnetic field and its properties have been experimented and interpreted since the 18th century, the following is a brief chronological overview of the main contributors of this field, representing the acknowledgment of their particularly important contribution to the technological benefits we experience today: **Michael Faraday** [1]; **Joseph Henry** [1]; **David Edward Hughes** [1]; **James Clerk Maxwell** [1]; **Sir Oliver Joseph** [1], [2]; **Nikola Tesla** [1], [3]; **Heinrich Rudolf Hertz** [1]; **Jagdish Chandra Bose** [1], [4]; **Aleksandr Stepanovici Popov** [1]; **Jozef Murgaš** [5]; **Guglielmo Marconi** [6], [7].

1.2 The current state of wireless power transfer development

In 2019, researchers from the Department of Wireless Energy at Imperial College, London, successfully tested a wireless charging drone, functioning in a new environment - at sea [9]. Also, in 2017 the Wärtsilä technology group successfully tested the first automated wireless charging system for a ferry in Norway [10]. Volvo Cars is integrating and testing new wireless charging technology in a real urban environment for future electric cars [11].

The first stage of WPT use in the marketplace has been powering the phones and tablets niche since 2012, with a market growth of around $1 billion, in 2015. In 2022 the WPT division was estimated at a market value of five billion dollars with a foreseeable increasing interest in the automotive and industrial areas [8].

1.3 State the challenge and research objectives

The main objectives of this PhD thesis are to design, realize and improve a WPT system of an independent base used to power naval aerial drones.
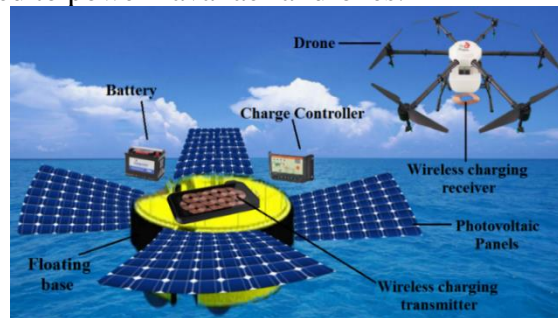
Fig. 1.1. The floating base overview (with a renewable energy source) used for wireless charging naval aerial drones [15]

The research aims to realize the concept of a Wireless Energy Transfer System, the one shown in Figure 1.2.
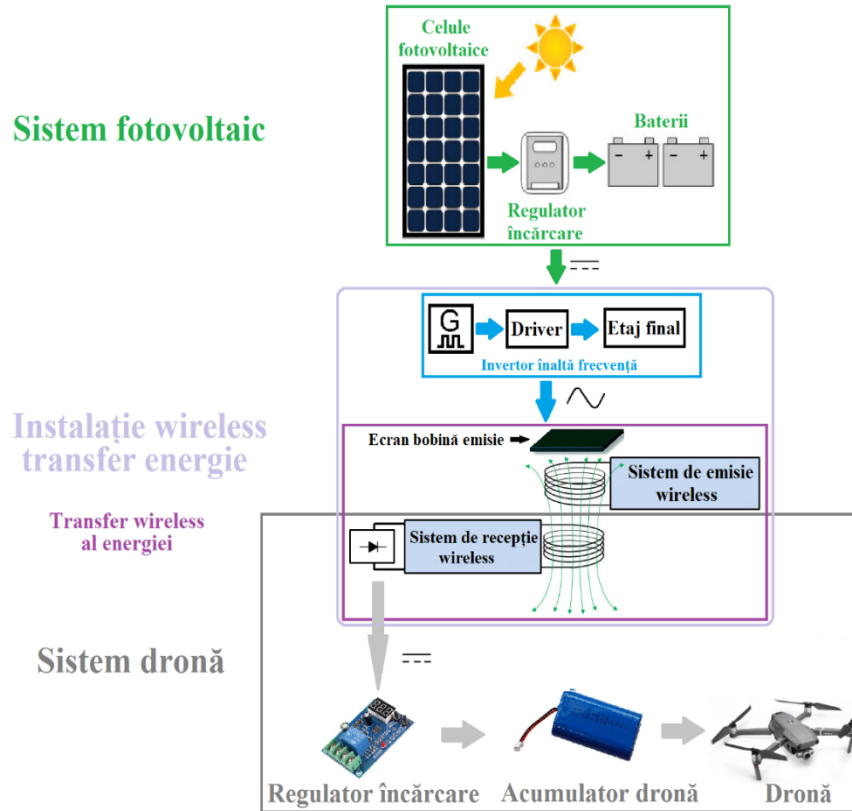
Fig. 1.2. The general concept of the autonomous aerial drone power supply base

In order to increase the efficiency and transferred power of the naval drone wireless power system, the following research guidelines will be followed.

High-frequency inverter

Study and simulation of inverters used in wireless power transfer in order to choose the optimal design.

Mutual resonant inductive coupling of two coils used in WPT

Mathematical modeling of two mutually coupled coils belonging to a wireless transfer system.

Coils used in wireless power transfer

Defining the parameters of planar loop coils and planar spiral coils, the adjustment, design, and exact establishment of equations used for calcuating the mutual and self-inductances by comparing the results with actual measurements for validation.

Shields used in wireless energy transfer

Experiments on the use of shield versions made of materials with different electrical and magnetic properties and the development of the sandwich shield concept for magnetic field reflection.

Determine the overall wireless transfer efficiency

The overall DC to AC conversion efficiency, wireless transfer, AC to DC conversion determining, powering the receiving circuit load using different resistances to determine critical coupling and maximum transfer efficiency.

1.4 Energy dimensioning of the wireless drone charging base

The independent platform's electrical energy required to power the aerial drone can be obtained from a variety of unconventional sources, the most practical seems to be the photovoltaics one.

The energy balance of the charging base PV system is designed in relation to the energy requirements of the drone.

Thus, to be able to provide some charge cycles for the drone, the storage capacity of the batteries must be related to the average solar exposure time of the PV panels [15]. An energy balance has to be performed for:

-Drone energy system,
-Photovoltaic (PV) module battery system,
-Photovoltaic panel battery voltage and charge regulator system,
-Photovoltaic panel system.

An important element for photovoltaic panel dimensioning is the number of hours of sunshine per day (24h). Along the Romanian coast, the average is shown in Table 1.1 [20].

Tabel 1.1. The monthly average no. of hours of sun exposure on the Constanta coast

Month	Jan	Feb	Mar	Apr	May	Jun	Jul	Aug	Sep	Oct	Nov	Dec
Hours	3	4	5	6	9	9	11	10	8	5	3	3

The darkest scenario should be considered, as the photovoltaic panels should cover the energy consumption needs given 3 hours of energy production time.

1.5 Wireless energy transfer phenomena

To get an overview of both the propagation phenomena of electromagnetic waves and the design characteristics of the transmitting and receiving coils and also of the inverter, an experiment was carried out before the research conducted in this paper. This sub-chapter represents introductory research on efficiency improvement and optimization of WPT.
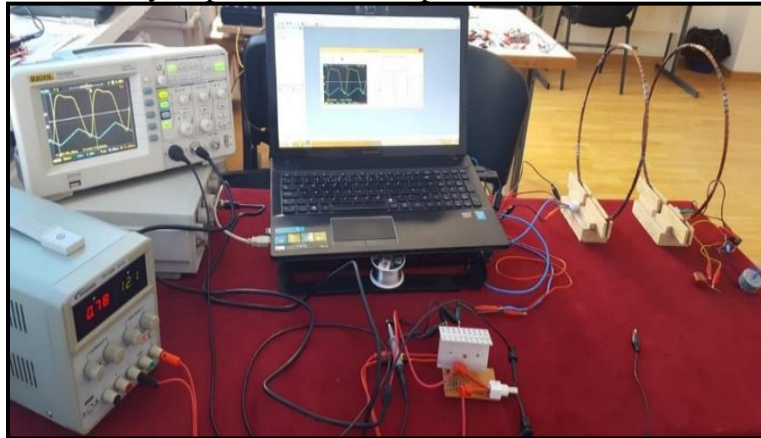

Fig. 1.3. The overview of the WPT system using a class E inverter [24]

This experiment consists of supplying an LC resonant oscillator circuit from a high-frequency mono-alternance voltage source and observing the variation of the WPT efficiency as the ratio between the energy consumed in the transmission coil and the energy received in the reception coil.

Results and discussion

To determine the best wireless power transfer efficiency, different waveforms with different frequencies are used, resulting in three experiments.

In experiment 1, the transmiting coil is supplied at a frequency of f=17.86 kHz, and a transfer efficiency of about 91% is obtained, the best result of all experiments in this chapter.

In experiment 2, to show the clear influence of voltage waveform on wireless transfer efficiency, the transmiting coil is supplied with the same frequency as in experiment 1 (17.86 kHz), but a different voltage waveform was used. The waveform of the voltage in experiment 2 shows less attenuation of the positive alternation period compared to experiment 1. In experiment 2, a transfer efficiency of about 45% was obtained, the lowest of all experiments in this chapter.

In experiment 3, the influence of frequency on transfer efficiency is revealed by supplying the transmitter coil with a voltage of approximately the same waveform as in experiment 1 but with a lower frequency, of 12 kHz, resulting in a transfer efficiency of 79%.

To perform a comparative study of the waveform parameters of the transmitter coil supply voltage, the experiments with the highest efficiency (experiment 1) and the lowest efficiency (experiment 2) were chosen, the waveform parameters of the voltages are shown in Figures 1.4, 1.5.

Fig. 1.4. Supply voltage waveform parameters for experiment 1
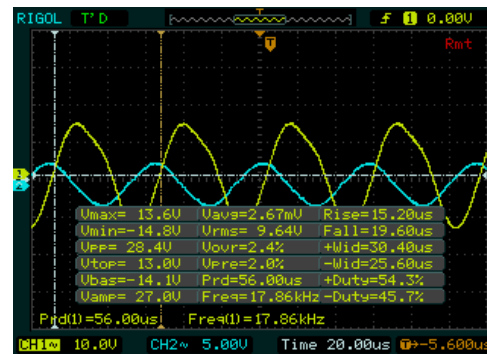
Fig. 1.5. Supply voltage waveform parameters for experiment 2

In experiment 1, the corresponding periods for Rise and Fall are significantly reduced and almost equal, compared to experiment 2. Referring to the +Wid and -Wid periods, in experiment 1 the +Wid/-Wid ratio ≈ 2.2 compared to experiment 2, where the +Wid/-Wid ratio ≈ 1.18.In experiment 1, the parameters +Duty and -Duty have a double ratio on the positive versus negative alternation, compared to experiment 2, where the ratio is almost equal.

1.6 Conclusions

According to the three experiments, the propagation efficiency of electromagnetic waves depends on several aspects of the transmitter coil supply voltage waveform:

- the shorter the transition periods (Rise, Fall) of the emission voltage waveform, the higher the efficiency of wireless power transmission;

- the longer the propagation period of one alternation (+Wid or -Wid) compared to the other alternation, the more efficiently the electromagnetic waves propagate through the air (this is influenced by the duty cycle).

- the more harmonics an alternation contains (without reversing the polarity of the alternation), the more efficient the propagation will be on that alternation, due to the continuous variation of the voltage.

2. THEORETICAL STUDY OF WIRELESS ENERGY TRANSFER

2.1 Introduction

Wireless power transfer systems categories

The first classification of wireless power transfer methods is the two types of fields, near and far, as shown in Figure 2.1 [33].
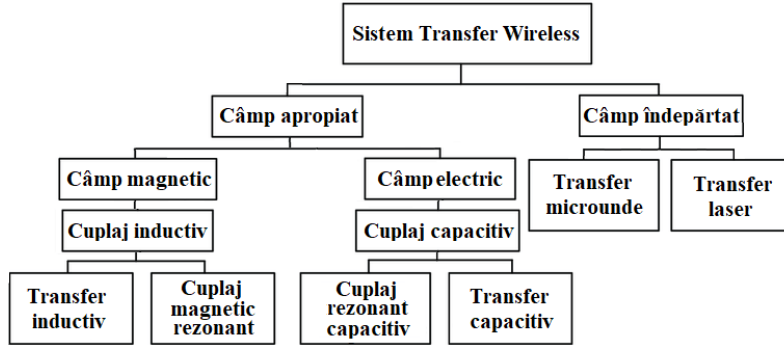
Fig. 2.1. Clasificarea tipurilor de transfer wireless [33]

Considering the specifics of this PhD thesis, the wireless near-field magnetic energy transfer will be used, as shown in Figure 2.1.

2.2 Mathematical modeling of the equivalent circuit associated with wireless energy transfer

Wireless power transfer by resonant magnetic circuits

For wireless energy transfer, the resonant magnetic coupling between LC oscillating circuits belonging to the primary (transmission or source) circuit and the secondary (receiving) circuit will be used, which can be configured in four topologies as shown in Figure 2.2.
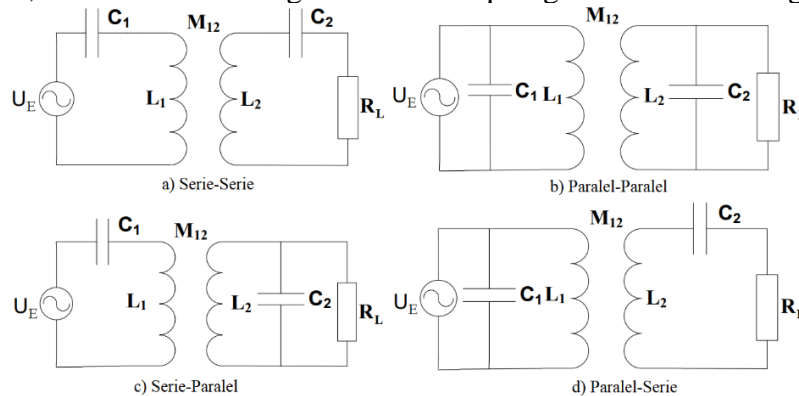
Fig. 2.2. Topologies of magnetically resonant coupled oscillating circuits [43]

The equivalent circuit of magnetically resonant coupled oscillator topologies

For a uniform approach to all types of magnetically coupled circuits, the Figure 2.3 diagram, generalizes the different connection topologies [43], [44].
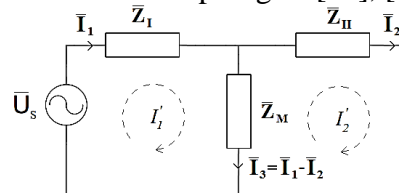
Fig. 2.3. Type T equivalent quadripol [43], [44]

After defining the two circuits' reflected impedances (primary and secondary), they are inserted into the two circuits diagram, as shown in Figure 2.4.
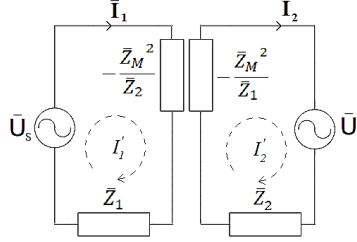
Fig. 2.4. Reflected impedances of mutually coupled oscillating circuits [46]

New equivalent diagrams are revealed in relation to the primary and secondarycircuits as presented in Figure 2.5, we can conclude that the influence of the primary to the secondary and vice versa is manifested by reflecting resistances ($R_{1\rightarrow 2Ref}$, $R_{2\rightarrow 1Ref}$) and reactances ($X_{1\rightarrow 2Ref}$, $X_{2\rightarrow 1Ref}$).
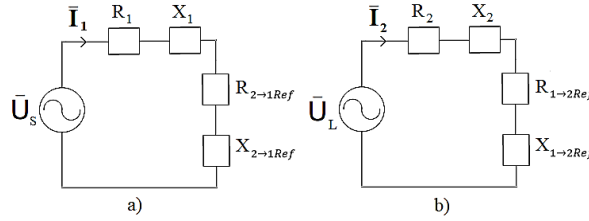
Fig. 2.5. Equivalent circuits involving reflected reactances and resistances

It can be concluded that the power consumed in the primary, on the resistance reflected by the secondary, represents the power transferred into the secondary circuit, and has the following expression:

$$P_2 = \frac{1}{2} R_{2\rightarrow 1Ref} I_1^2 \qquad (2.1)$$

where: P_2 - transferred power to the secondary circuit.

After the power P_2 determination, the total power can be expressed as follows:

$$P = P_1 + P_2 = \frac{1}{2} R_1 I_1^2 + \frac{1}{2} R_2 I_2^2 \qquad (2.2)$$

where: P_1 - consumed power in the primary circuit.

2.3 Maximum power transfer condition

For magnetic mutual coupling, the critical coupling coefficient is defined as:

$$k_{crt} = \frac{X_{Mcrt}}{\sqrt{X_1 X_2}} = \frac{\sqrt{R_1 R_2}}{\sqrt{\omega L_1 \omega L_2}} = \frac{1}{\sqrt{Q_1 Q_{2tot}}} \rightarrow k_{crt} Q_k = 1 \qquad (2.3)$$

Maximum power transfer for reception is achieved when the maximum secondary current I_{2MM} is reached:

$$P_{2MM} = \frac{1}{2} R_1 I_1^2 = \frac{1}{2} R_1 \frac{U_1^2}{\left(R_1 + R_{2\rightarrow 1Ref}\right)^2} = \frac{1}{2} \left(\frac{U_1^2}{4R_1}\right) \qquad (2.4)$$

2.4 Maximum power transfer efficiency

The power transfer efficiency of coupled circuits will be expressed as the ratio between the power received in the secondary P_2 and the total power P [39], [49], [48]:

$$\eta = \frac{P_2}{P} = \frac{R_{2\to1Ref}I_1^2}{(R_1 + R_{2\to1Ref})I_1^2} = \frac{R_{2\to1Ref}}{R_1(1 + \frac{R_{2\to1Ref}}{R_1})} = \frac{\frac{R_{2\to1Ref}}{R_1}}{1 + \frac{R_{2\to1Ref}}{R_1}} \tag{2.5}$$

therefore, respecting the specific equality of maximum power transfer $(R_1 = R_{2\to1Ref})$, the expression of the efficiency becomes:

$$\eta = \frac{1}{2} = 50\% \tag{2.6}$$

2.5 The maximum transfer efficiency in terms of load resistance

The total transfer efficiency from the primary circuit to the load is defined as [49], [50]:

$$\eta_{tot} = \eta_Q\eta_2 = \frac{k^2Q_1Q_{2tot}}{1 + k^2Q_1Q_{2tot}}\left(\frac{Q_2}{Q_L + Q_2}\right) \tag{2.7}$$

The optimal load resistance of the secondary circuit $R_{L_{opt}}$ is calculated (related to the coupling coefficient k):

$$\frac{Q_2(Q_2 + Q_L)}{Q_2 + Q_L + k^2Q_1Q_2Q_L} = Q_L \to Q_2^2 + Q_2Q_L = Q_2Q_L + Q_L^2 + k^2Q_1Q_2Q_L^2 \to$$

$$Q_{L_{opt}} = \frac{Q_2}{\sqrt{1+k^2Q_1Q_2}} \text{ [50]} \tag{2.8}$$

the optimal load quality factor of the secondary circuit can have values of: $Q_{L_{opt}} \geq 0$.

2.6 The coupled circuits resonance

Typically, in the case of mutually coupled circuits for wireless power transfer, it is intended that the value of the current in the secondary circuit to be maximum, which also ensures a maximum transferred power, this condition (maximum current in the secondary) is achieved by tuning the circuits to resonance.

2.7 Defining the equations of mutually coupled circuits (series-series, parallel-parallel)

As a study of near-field wireless energy transfer, the operating equations of the mutual inductive coupling of the two oscillating transmit-receive circuits will be determined.
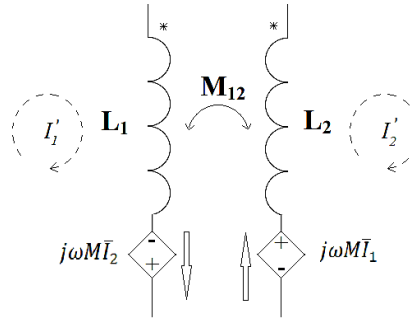
Fig. 2.6. The mutual influence of two coils [47]

From Figure 2.6, L_1 and L_2 - represent the transmit and receive coils in which currents $\bar{I}_1$ and $\bar{I}_2$ flow, the coils are mutually influenced by mutual inductance M; the coils have the same winding/polarization direction, marked with *. The current $\bar{I}_1$ in L_1 will induce a voltage $(j\omega M\bar{I}_1)$ in L_2, opposite to the voltage applied on L_1 and consequently a current $\bar{I}_2$. In return, $\bar{I}_2$ will induce a voltage $(j\omega M\bar{I}_2)$ in L_1 opposite to the voltage induced in L_2 [51], [52].

Applying the equivalent T-type quadrupole theory from figure 2.3, a universal circuit can be created for any type of inductive mutual coupling (series-series, series-parallel, parallel-series, parallel-parallel) as shown in figure 2.7, (equivalent impedances $\bar{Z}_{1e}$ and $\bar{Z}_{2e}$).
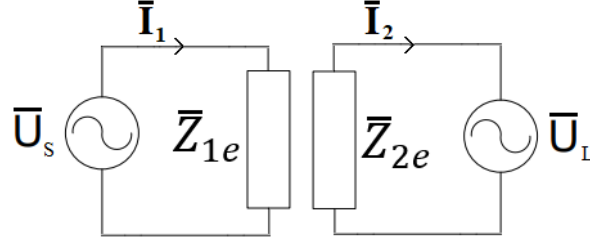
Fig. 2.7. The equivalent transmitting and receiving circuit schemes

2.8 Forced oscillations in series and derivation circuits
The voltages resonance, overvoltages [39], [56], [57]

At resonance, the voltages of the coil and capacitor's (series) terminals are equal in magnitude but vary in antiphase. At the terminals of L and C overvoltages occur $U_L = U_C = Q_{serie}U$, so the series RLC circuit at resonance will amplify Q_{serie} times the voltage applied to the circuit terminals.

$$Q_{serie} = \frac{L\omega_0}{R} = \frac{1}{C\omega_0 R} \qquad (2.9)$$

The currents resonance, overcurrents [38], [56], [57]

At resonance, the I_L and I_C currents have almost equal amplitudes and are shifted by about 180°.

$$\frac{I_C}{I} = \frac{I_L}{I} = Q_{parallel}, Q_{parallel} = \frac{R}{L\omega_0} \qquad (2.10)$$

Therefore, the derivation circuit amplifies at resonance with $Q_{parallel}$ several times the source current.

2.9 Conclusions

The study in this chapter has demonstrated and theoretically substantiated two approaches to wireless energy transfer with economic and technical implications:
- maximum power transfer (defined by critical coupling),
- maximum transfer efficiency (defined by optimal load resistances).

For the transfer efficiency, two theoretical calculation alternatives were demonstrated:
- making power ratio,
- involving the coupling coefficient and the circuit quality coefficients.

At the same time, the exact equations necessary for the calculation were defined and demonstrated: the optimal resistivity for maximum efficiency, the critical coupling, and the maximum current in the reception circuit.

3. COILS USED IN WIRELESS POWER TRANSFER

3.1 Phenomena and characteristics associated with coils

The conductor length used in coil construction

The conductor length used in the flat spiral coil winding is determined using Gauss's formula as follows:

$$l_s = 2\pi \left[Nr_i + \left(\frac{(N-1)N}{2} \right)(w+p) \right]$$ (3.1)

where: l_s - conductor length used in the construction of a flat spiral coil, w - conductor diameter, p - space between turns.

The conductor length used in the planar loop coil winding is calculated using the average diameter of the coil as follows:

$$l_b = N2\pi \left(\frac{D_o + D_i}{2} \right)$$ (3.2)

where: l_b - conductor length used in the construction of a planar loop coil, D_o - outer coil diameter, D_i - inner coil diameter.

Coil resistance

The total resistance of a coil used in wireless power transfer is the sum of the AC resistance including the proximity resistance and the skin effect [61].

$$R_a = R_{skin} + R_{prox}$$ (3.3)

where: R_a - total resistance of the coil supplied at high frequency AC , R_{skin} - resistance due to skin effect, R_{prox} - proximity resistance.

Skin effect resistance
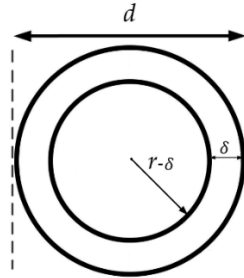
Fig. 3.1. Conductor cross-section and the alternating current depth of penetration δ [61]

The coil's conductor diameter used in high-frequency alternating current is subject to the limitation of the current penetration depth δ, as follows:

$$R_{skin} = \frac{l}{\sigma[\pi r^2 - \pi(r-\delta)^2]} = \frac{l}{\sigma[\pi(2r\delta - \delta^2)]} \rightarrow$$ (3.4)

the relationship must be satisfied $2r\delta - \delta^2 > 0 \rightarrow \delta(2r - \delta) > 0$, such as:

$$2r > \delta$$ (3.5)

To calculate the AC resistance for a Litz conductor, the equation is:

$$R_{skin \, (Litz)} = \frac{l}{\sigma[\pi(n2r\delta - \delta^2)]}$$ (3.6)

Proximity resistance

Equivalent currents, induced by the magnetic field's strength, are positioned on the conductor's surface and the current distribution is no longer symmetricaly circular [65].
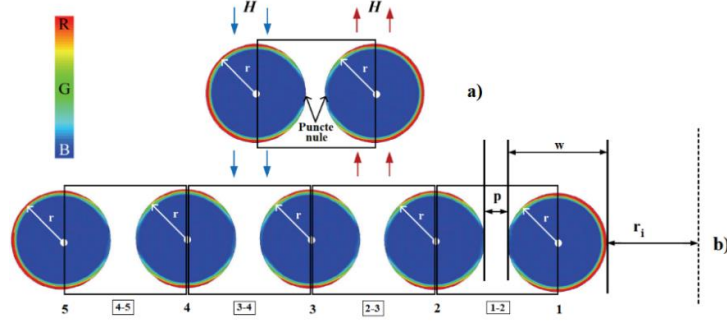
Fig. 3.2. Association between the interaction of two conductors and a sequence of conductors in a single-layer planar spiral coil [65].

To simplify the proximity resistance calculation between the conductors of a planar spiral coil, an association (N) has been made with the interaction of two conductors passed through by the same current in terms of the effect in each half section.

The proximity resistance between two parallel conductors passed by the same current is:

$$R_{prox} = [2\frac{1}{\sigma S}\pi^2 r^2 \left(\frac{2r}{\delta} - 1\right)]H^2 \ (\Omega * m) \tag{3.7}$$

where: H - magnetic field strength.

We can define the total length equation of conductors under the proximity resistance:

$$l_{tot} = \frac{2\pi[2(N-1)r_i + (w+p)\left\{2\left(\frac{(N-2)(N-1)}{2}\right) + (N-1)\right\}}{2} \tag{3.8}$$

In order to eliminate the proximity effect between the coil turns and neglect it in the calculations, an optimal ratio between the space between the conductors and their radius must be achieved:

$$p/r \tag{3.9}$$

where: p - space between conductors, r - conductor radius. This optimal ratio is demonstrated in the paper [70] and shown in Figure 3.3.
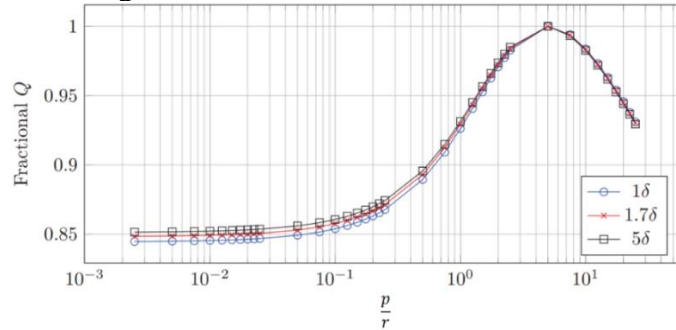
Fig. 3.3. The optimal ratio for maximum quality factor [70]

3.2 The self and mutual inductances equations

The assumption of **mutual inductance calculation** between two coils at a distance h from each other, for planar spiral and planar loop coils, both with concentric circular turns, starts from a basic equation calculating the mutual inductance of two coils with one turn each of radius R_i and R_j at a distance h [76]:

$$M\left(R_i, R_j, h\right) = \mu_0\sqrt{R_i R_j}\left[\left(\frac{2}{s} - s\right)K(s) - \frac{2}{s}E(s)\right] \tag{3.10}$$

where: M - mutual inductance of two coils formed by one turn each, R_i - radius of the transmitting coil of order i, R_j - radius of the receiving coil of order j, s - variable depending on de R_i, R_j, h, $K(s)$ and $E(s)$ - complete elliptic integrals of degree I and II.

It will be noted that in the case of mutual inductance the conductor radius (r) is neglected since $\frac{r}{R} \ll 1$. The calculation of the mutual inductance between two coils containing more than one turn is performed by the following equation [76]:

$$M_{i,j} = \sum_{i=1}^{N_i} * \sum_{j=1}^{N_j} M(R_i, R_j, h) \rightarrow \tag{3.11}$$

where: $M_{i,j}$ - the mutual inductance of the multispiral coils, the number of turns has the following values - $i=1,2,...N_i$ and $j=1,2,...N_j$, $i \neq j$.

The self-inductance calculation hypothesis for planar spiral and planar loop coils, both with concentric circular turns, satisfying the condition $\frac{r}{R} \ll 1$, starts from a basic equation calculating the self-inductance of a single spiral coil of radius R [75], [77]:

$$L(R,r) = \mu_0 R (\ln \left(\frac{8R}{r}\right) - 2) \tag{3.12}$$

where: R - radius of the coil in the emission/reception, r - radius of the conductor in the emission/reception coil.

In order to demonstrate the applicability and accuracy of the equations, all theoretical inductance results determined by the calculation equations/software will be verified by real coil inductance measurements.
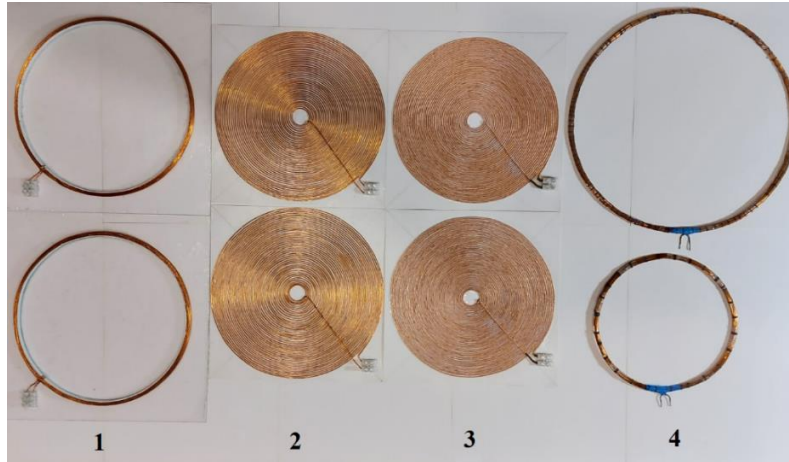
Fig. 3.4. Coils used in the wireless power transfer study: 1,4 - planar loop coils, 2 - planar spiral coils with the solid conductor, 3 - planar spiral coils with the Litz conductor [78]

3.2.1 Planar loop coils

The self-inductance for a planar loop coil with N turns is calculated by multiplying equation (3.32) by the square number of turns, and is defined as follows [76], [79]:

$$L(r,w) = \mu_0 N^2 R (\ln \left(\frac{8R}{r}\right) - 2) \tag{3.13}$$

Another equation for determining the self inductances for a mono spiral coil (expressed in Henry) inspired by the paper [39] is:

$$L(R,r) = 2\pi\mu_0 D (\ln \left(\frac{D}{r}\right) - 0.33)10^{-1} \tag{3.14}$$

The adaptation of this equation to multi-turn planar loop coils can be done by multiplying the equation by the number of turns N, not by the square number of turns N^2, so the equation becomes:

$$L(R,r) = N2\pi\mu_0 D\left(\ln\left(\frac{D}{r}\right) - 0.33\right)10^{-1} \tag{3.15}$$

The difference between the value of the inductance calculated using equation (3.13) and the measured one is:

coil A, 85.11µH-69.1µH=15.71 µH, this resulted in an increase of measured value by 23.17%,
coil B, 53.28 µH-45.1 µH=8.18µH, this resulted in an increase of measured value by 18.14%,
coil C, 193.05µH-165.8µH=27.25µH, this resulted in an increase of measured value by 16.43%.

The difference between the value of the inductance calculated using equation (3.15) and the measured one is:

coil A, 111.79µH-69.1µH=42.69µH, this resulted in an increase of measured value by 69.1%,
coil B, 69.27 µH-45.1 µH=24.17µH, this resulted in an increase of measured value by 53.59%,
coil C, 164.53µH-165.8µH=-1.17µH, this resulted in an decrease of measured value by 0.76%.

Total mutual coupling of planar loop coils, made up of a sequence of N concentric turns of radii R_i(i=1....N_i and R_j(j=1.....N_j), having the following specific construction characteristics of the coil C: N1 = N2 =18, $R_i = R_j = 0.101$m, h = 0.015m. The mutual inductance value 9.6932e-05≈96.932µH (mutual inductance) was obtained for a coil spacing h=0.015m. By analogy with the calculation of self-inductance, the mutual inductance will be decreased by 16.43%.

3.2.2 Planar spiral coils

Before calculating the planar spiral coil's inductances, as shown in Figure 3.5, an equation for the turns radii calculation was defined.

$$R_{N_1} = r_i$$
$$R_{N_2} = r_i + (w + p) \rightarrow R_{N_n} = r_i + (w + p)(N - 1) \tag{3.16}$$

where: r_i - inner coil radius, R_N - spiral radius, w - conductor diameter, p - space between the coils.
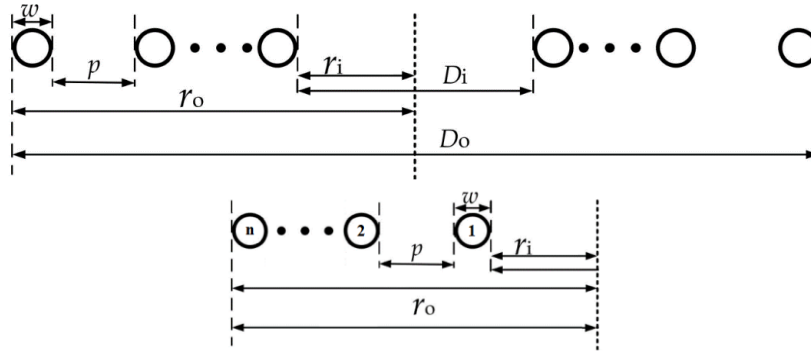
Fig. 3.5. The turns radii calculation of a planar spiral coil

The self-inductance for a planar spiral coil formed by a sequence of N concentric turns of different radii R_i (i=1,2,....N) and conductor radius r, satisfying the condition $\frac{r}{R} \ll 1$, is defined as follows [76]:

$$L_{tot} = \sum_{i=1}^{N} \mu_0 r_i\left(\ln\left(\frac{8R_i}{r_i}\right) - 2\right) + \sum_{i=1}^{N_i} {}^* \sum_{i\neq j}^{N_j} \mu_0\sqrt{R_i R_j}\left[\left(\frac{2}{s} - s\right)K(s) - \frac{2}{s}E(s)\right] \tag{3.17}$$

where: L_{tot} - coil inductance, i≠j.

It should be remembered when calculating this self-inductance that the i and j turns are of the same coil, and the definition of the mutual inductance in equation (3.17) is done by defining the mutual couplings between the turns of the same coil defined as i and j in order to make combinations of i, j couplings.

Another equation for determining the self-inductance (in µH) for a planar coil (dimensions in inches) is [80]:

$$L = \frac{A^2 N^2}{30A - 11D_i}$$
$$A = \frac{D_i + N(w + p)}{2}$$

(3.18)

where: D_i - inside diameter of the coil.

Calculations according to equation (3.18) gave the following self-inductance results:
- **coil D:** 161.74 µH,
- **coil E:** 156.27µH.

In order to check the accuracy of the equation's results, the inductance of the two planar spiral coils was measured, as shown in Figure 3.6, using an RLC Meter.

Fig. 3.6. Checking planar spiral coil self-inductance (coil type D, E)

The following self-inductances were obtained from the measurements:
- **coil D:** 165.6µH,
- **coil E:** 157.3µH.

The difference between the inductances calculated using equation (3.17) and the measured ones are:
coil D: 202.7µH-165.6µH=37.1 µH, this resulted in an increase of measured value by 22.4%,
coil E: 195.3µH-157.3µH =38µH, this resulted in an increase of measured value by 24.16%.

The difference between the inductances calculated using equation (3.18) and the measured ones are:
coil D: 161.74µH-165.6µH=-3.86µH, this resulted in an decrease of measured value by 2.33%,
coil E: 156.27µH -157.3µH =-1.03µH, this resulted in an decrease of measured value by 0.65%.

Mutual coupling of planar spiral coils made up of a sequence of N turns of radii R_i(i=1....N_i and R_j (j=1..... N_j), each coil having different radii for each turn, with the following construction characteristics specific to variant D:
- N1 = N2 =44,
- ri1 = ri2 = 0.0095m,
- w(i) = w(j) =0.001,
- p(i) = p(j) = 0.0011,
- h=0.015m.

A mutual inductance of 8.1740e-05≈81.74µH was obtained for a coil's spacing h=0.015m. By analogy with the calculation of self-inductance, the mutual inductance will be decreased by 22.4%. Thus for h=0.015m, the theoretical mutual inductance will be ≈ 63.44µH, defining a coil coupling coefficient of k=0.37.

3.3 Manufacture of coils and final characteristics determination

For the practical realization of the coils, two types of copper wire enamelled separately (with polyurethane enamel) of different diameters will be used:
- 1 mm solid conductor,
- 1.2 mm Litz conductor (made by twisting 25 conductors of 0.2 mm diameter).

Two approximately identical coils were made for each type C, D, E, with the characteristics shown in Table 3.1. for the next experiments in the following chapters.
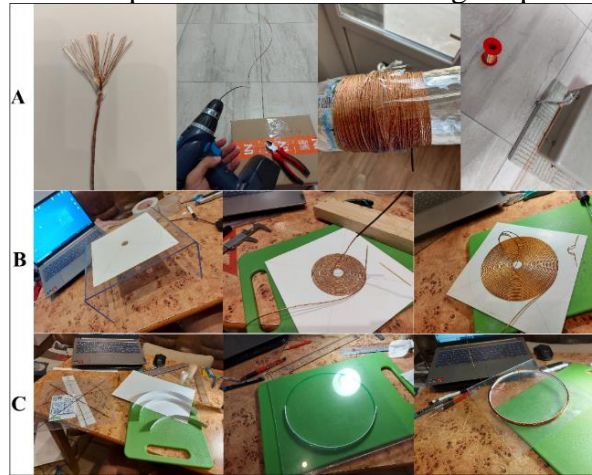
Fig. 3.9. Coil construction: A - Litz conductor,
B - planar spiral coils, C - planar loop coils

Tabel 3.1. Coils specifications C, D, E

No.	Type	Turns no.	Di	Do	w	p	Conductor length (m)	Coil type	
1	D	44	0.019	0.203	0.001	0.0011	15.39	Solid conductor	Planar spiral coil
2		44	0.019	0.209	0.001	0.00116	15.76		
3	E	44	0.019	0.196	0.0012	0.0082	14.91	Litz Conductor	
4		44	0.019	0.195	0.0012	0.008	14.79		
5	C	18	0.202	-	0.001	-	11.42	Solid conductor	Planar loop coil
6		18	0.202	-	0.001	-	11.42		

Coil quality factor in terms of construction type and power supply frequency

Six coils (pairs of two with almost identical dimensions) will be compared, the dimensions of which are shown in Table 3.1. Using an RLC Meter the inductance, DC resistance and quality factor will be measured for different frequencies (1kHz, 10kHz, 100kHz), the results are shown in Table 3.2.

Tabel 3.2. Coil parameters for different power supply frequencies: 1kHz, 10kHz, 100kHz

No.	Planar spiral coil (solid conductor)		No.	Planar spiral coil (Litz type conductor)		No.	Planar loop coil (solid conductor)	
1	**L=165.6µH**	**Rdc=0.38 Ω**	**3**	**L=165.3µH**	**Rdc=0.38 Ω**	**5**	**L=162.5µH**	**Rdc=0.29 Ω**
	f (kHz)	Q		f (kHz)	Q		f (kHz)	Q
	1	2.84		1	2.9		1	3.7
	10	26.2		10	27.3		10	25.5
	100	126		100	257		100	54.3
2	**L=174.1µH**	**Rdc=0.4 Ω**	**4**	**L=157.3µH**	**Rdc=0.36 Ω**	**6**	**L=165.8µH**	**Rdc=0.3 Ω**
	f (kHz)	Q		f (kHz)	Q		f (kHz)	Q
	1	2.87		1	2.82		1	3.75
	10	26.5		10	25.3		10	27.3
	100	126		100	235		100	53.2

3.4 Conclusions

Following the experiments in this chapter, we can conclude the following:

Even if the equations for calculating the self-inductance for loop or planar spiral coils (3.13) and (3.17) are mentioned and used in many literature articles (in the field of wireless energy transfer [76], [60], [81], [82], [83], [84]), they do not apply to calculations in the field of wireless energy transfer, where the coils do not respect the condition of the conductor diameter to coil diameter ratio ($\frac{r}{R} \ll 1$), the equations being taken on from the field of radio engineering.

The total cross-section of the Litz-type conductor of coil E is the same as the cross-section of the conductor of coil D, the space allocated to a turn as well as the geometry of the coils (inner diameter and outer diameter) being approximately identical between the two coils D and E, which shows that the nature of the conductor does not influence the inductance, as long as the geometrical parameters listed in the paragraph are respected; variant D having a larger space between the turns also resulted in a proportionally larger outer diameter and inductance than variant E.

Regarding the mutual inductance (for planar loop and planar spiral coils): if identical coils are used in both transmission and reception, the error found in the case of the self inductances calculated by equations (3.13) and (3.17) - 16.43%, 22.4%, compared to the equations that gave exact results, is subtracted from the mutual inductance for correction.

From the study of the quality factor of the coils in Table 3.2 we can conclude the following: at low frequencies up to 10kHz the quality factor Q is almost identical for all 6 coils, thus the type of conductor (Litz or solid) or the type of coil (spiral or loop) have no significant influence. With the increase of the power supply frequency of the coils to 100kHz, as expected, the planar spiral coil made of Litz type conductor obtained a much higher quality factor than the other planar spiral coils using solid conductor, about Q≈240 (100% higher), which recommends them for use in wireless systems operating at frequencies above 100kHz. Planar loop coils with solid conductors obtained 80% lower Q values than planar spiral coils with Litz conductors (for f=100kHz). In terms of quality coefficient, for low frequencies of around 10kHz solid coils are recommended, as they have a robust, and simple construction.

4. INVERTERS USED IN WIRELESS POWER TRANSFER

This chapter presents a simulated study of inverters used in wireless power transmission: H-bridge inverter, half-bridge inverter, E-class inverter.

4.1 Simulation of experimental inverter models

Two types of converters can be used to power oscillating circuits designed for wireless power transfer: DC-A.C. or DC-DC (semi-alternating signal) powering LC (series or parallel) oscillating circuits designed for wireless power transfer.

4.1.1 Full bridge H inverter

The H-bridge inverter component consists of four switching elements with two inverted signal outputs (Low and High), as shown in Figure 4.1.

Fig. 4.1. Full bridge H inverter

4.1.2 Half bridge inverter

The half-bridge inverter component consists of two switching elements with two inverted signal outputs (Low and High), as shown in Figure 4.2.
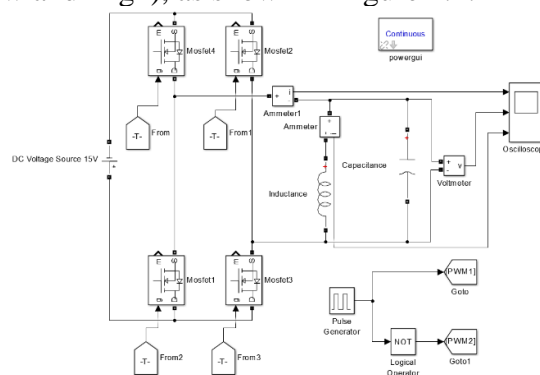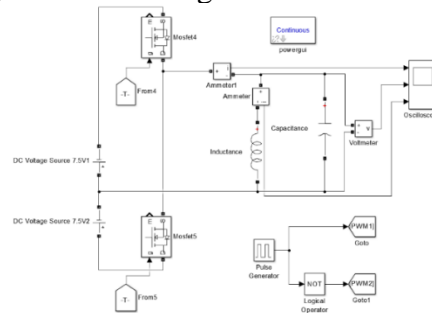

Fig. 4.2. Half bridge inverter

4.1.3 Class E inverter

The Class E inverter component consists of a switching element, as shown in Figure 4.3.
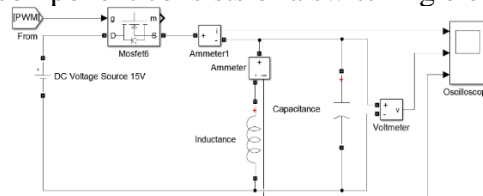

Fig. 4.3. Class E Inverter

4.2 Conclusions

Following the simulations carried out on the operation of the inverters, the data obtained has been summarised in Table 4.1 for interpretation and conclusioning.

Tabel 4.1. Inverter simulation data centralizer

Inverter type	Resistive load				
Full bridge H inverter	I_{rms1}	U_{rms1}	P_1	$THD_{curent1}$	$THD_{tensiune1}$
	0.608A	13,38V	8.135W	47,71%	47,71%
Half bridge inverter	I_{rms3}	U_{rms3}	P_3	$THD_{curent3}$	$THD_{tensiune3}$
	0.3055A	6.721V	2.05W	47,71%	47,71%
Class E inverter	I_{rms5}	U_{rms5}	P_5	$THD_{curent5}$	$THD_{tensiune5}$
	0.3055A	6.721V	2.05W	48,33%	48,33%

Inverter type	LC oscillating load - parallel						
Full bridge H inverter	I_{rms2}	U_{rms2}	P_2	$I_{rms\ bobină A}$	$THD_{curent2}$	$THD_{tensiune2}$	$THD_{curent\ bobină A}$
	0.84A	13.34V	11.2W	1.13A	215.94%	47,71%	12,13%
Half bridge inverter	I_{rms4}	U_{rms4}	P_4	$I_{rms\ bobină B}$	$THD_{curent4}$	$THD_{tensiune4}$	$THD_{curent\ bobină B}$
	0.53A	6.71V	3.56W	0.569A	52.16%,	47,56%	12,11%
Class E inverter	I_{rms6}	U_{rms6}	P_6	$I_{rms\ bobină B}$	$THD_{curent6}$	$THD_{tensiune6}$	$THD_{curent\ bobină C}$
	0.6A	18.41V	11.1W	1.501A	150.96%	52.4%	45,66%

Inverter type	RLC oscillating load - series					
Full bridge H inverter	$I_{curent2s}$	$U_{tensiune\ bobină2s}$	$U_{tensiune\ principală2s}$	$THD_{curent1s}$	$THD_{tensiune\ bobină1s}$	$THD_{tensiune\ principală1s}$
	5.72A	68.21V	6.12V	2.84%,	5.79%	52,73%
Half bridge inverter	$I_{curent2s}$	$U_{tensiune\ bobină2s}$	$U_{tensiune\ principală2s}$	$THD_{curent2s}$	$THD_{tensiune\ bobină2s}$	$THD_{tensiune\ principală2s}$
	5.67A	69.27V	6.16	3.66%,	5.94%	53,02% d
Class E inverter	-					

According to Table 4.1 we can conclude the following:

a.   resistive load

- unlike the H-bridge inverter, the half-bridge and E-class inverters obtained the same low values of voltage and current, with a slight increase in current and voltage THD for the E-class inverter,

- the H-bridge inverter achieved double the voltage and current values compared to the other two inverters, using all the energy of the voltage source, which recommends it over the other two inverters for powering resistive loads.

b.   Parallel LC load

- H-bridge inverter, provides the highest current through the coil, creating the strongest magnetic field, which is desirable for wireless magnetic induction transfer,

- Class E inverter, applies the highest voltage across the coil, which is recommended for wireless electric field transfer.

c.   Series RLC load

- The Class E inverter can not operate in this configuration because the DC output voltage, in theory, but also in simulation, can not pass through the series capacitor,

- in the case of full H-bridge and half-bridge inverters, an increase in the voltage applied to the coil is observed and therefore a much higher current flows through the coil, values which are significantly higher than in all experiments, which recommends them for supplying oscillating series RLC loads.

In terms of the power factor of inverter loads ($\cos(\varphi)$), it is influenced by the current THD, according to the paper [88]:

$$\text{Power factor} = \cos(\varphi)\sqrt{\frac{1}{1 + THD_{curent}^2}}$$

(4.1)

It is confirmed the theory from chapter 2.8:
- in the case of series LC oscillating circuits, the voltage applied to components L and C is amplified with respect to the generator voltage,
- in the case of parallel LC circuits, the current through the branches containing the L and C elements is amplified with respect to the main current at the inverter output.

We can thus confirm that the LC elements in the transmitter circuit must be connected in parallel if wireless transfer by magnetic induction is desired.

4.3 Inverters construction

Following the simulated theoretical study of inverters in the previous chapters [92], H-bridge and E-class inverters were selected for practical realization. Figure 4.4 shows the control topology of the inverters.
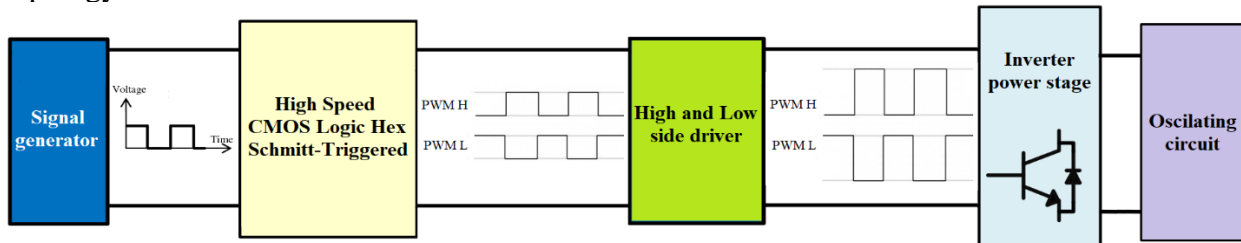
Fig. 4.4. The general topology of an H-bridge or E-class inverter used in practical realization in this paper [93]

4.3.1 Full bridge H inverter

For H-bridge inverters, MOSFET transistors with high side (H) and low side (L) switching are required.

Operation of MOSFET transistor drive using IR2112 driver [98], [100]

Control of the MOSFET transistor drivers is achieved by applying to the HIN and LIN inputs (belonging to IR2112) the signals Signal 1 and Signal 2 transmitted by CD74HC14 (Figure 4.5).
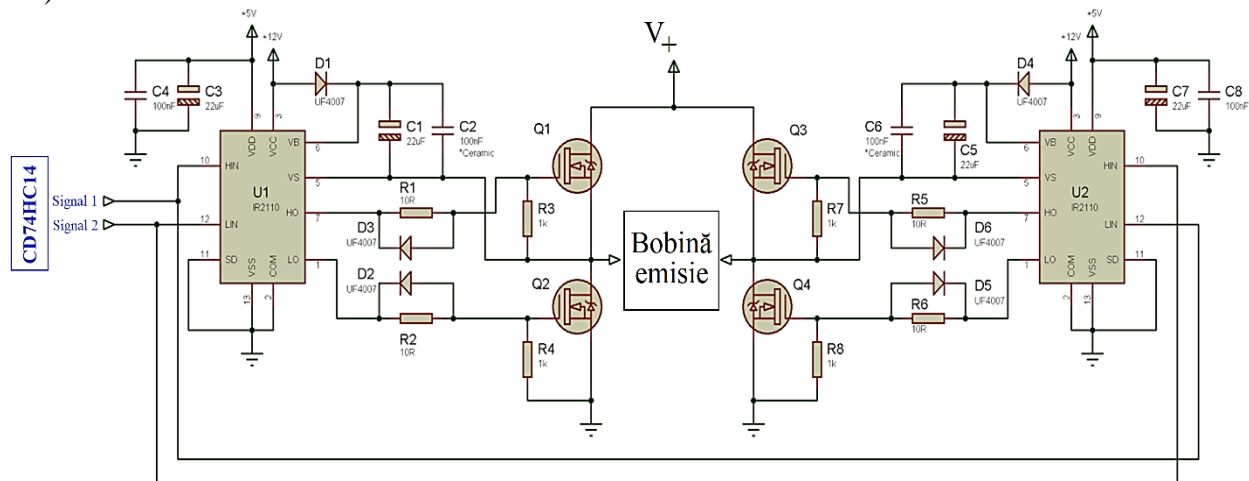
Fig. 4.5. Complete wiring diagram of the H-bridge inverter [100]

Component group D1, C1, C2 form the bootstrap circuit for U1 (IR2112) as do D4, C5, C6 for U2 (IR2112).

In order to simulate the full functioning diagram (appendix 1) not having power transistors assembled, a trick was consisting of : pins 5 (Vs) of the IR2112 drivers being connected to minus (as can be seen in figure 4.6) to charge the capacitors (bootstrap) was used.
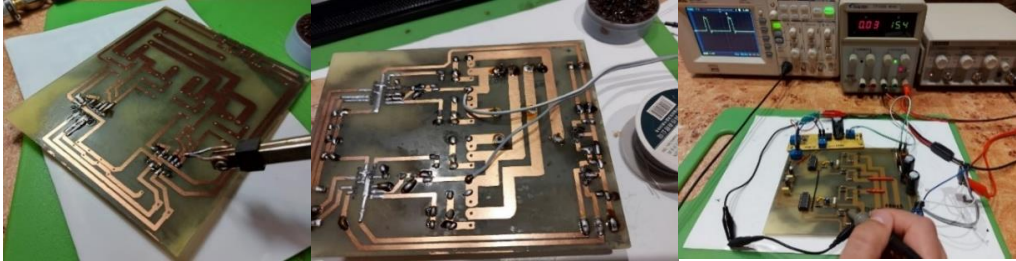
Fig. 4.6. Assembling H-bridge inverter board elements and testing without power transistors

The power transistors and cooling radiators were installed, the first functional tests were performed, the circuits were tinned and 1.5 mm^2 conductors were installed on the power circuits (Figure 4.7).
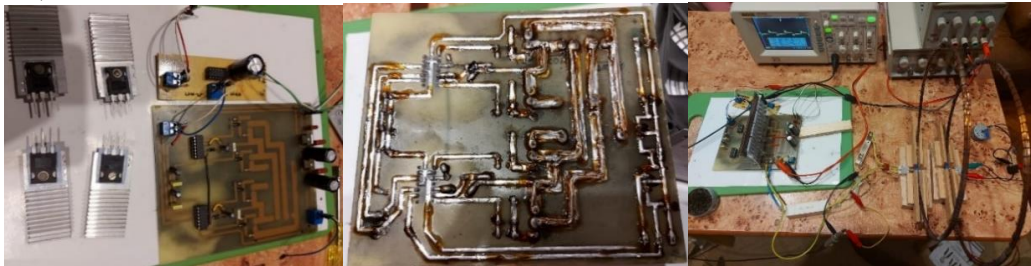
Fig. 4.7. Mounting of radiators, tinning and thickening of power circuits, H-bridge inverter testing

4.3.2 Class E inverter

The following figures 4.8 and 4.9 briefly present the stages in the verification and construction of Class E inverters.
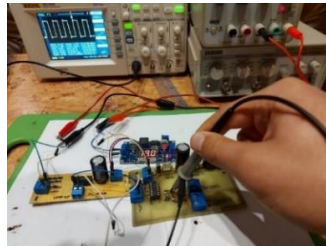
Fig. 4.8. Checking the IR2112 driver output signal without mounting the power transistor
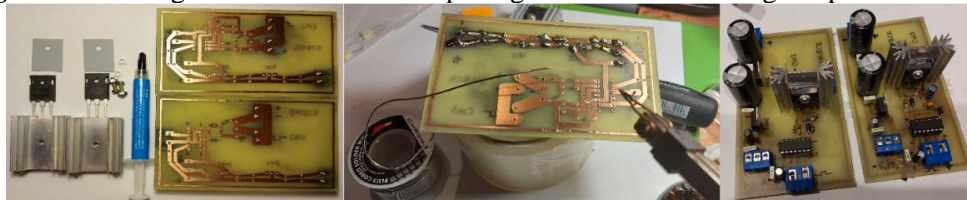
Fig. 4.9. Construction of class E inverters

4.4 Conclusions

Improving the square waveform and limiting voltage spikes at the output of the H-bridge inverter can be achieved by:
1. using a separate power supply for the control stages (hex inverters, drivers) from the power stage,
2. mounting a shock coil on the power stage supply circuit to limit current shocks,
3. installing RC or LC filters on the power supply of the control stages (hex inverters and drivers)
4. increasing the supply voltage of the drivers from 12VDC to 15VDC to reduce the switching losses of the MOSFETs (full open power transistors),
5. replacing the diode on the control input of the inverter hex with a fast diode and filtering the control signal with RC or LC filter.
6. mounting a 1 nF capacitor between the Gate control of the power transistors and ground.

Regarding the construction steps of the H-bridge inverter, it is very important to check the driver signals (LO and HO) before connecting the power transistors; an error in the timing of the power transistor control will cause irreversible damage to the inverter.

Another aspect related to the safety in the inverter operation is not to supply the power stage (power transistors) without activating its control.

In the practical experiments on efficiency and wireless transferred power in the following chapters the H-bridge inverter will be used, the study about the use of the E-class inverter being a future research premise.

5. OPTIMISATION OF MAGNETIC COUPLING SYSTEMS USING SHIELDS

5.1 Defining the properties of the shields used

The research in this chapter is based on conducting experiments to increase wireless power transfer efficiency by shielding and reflecting electromagnetic waves from the transmit coil.
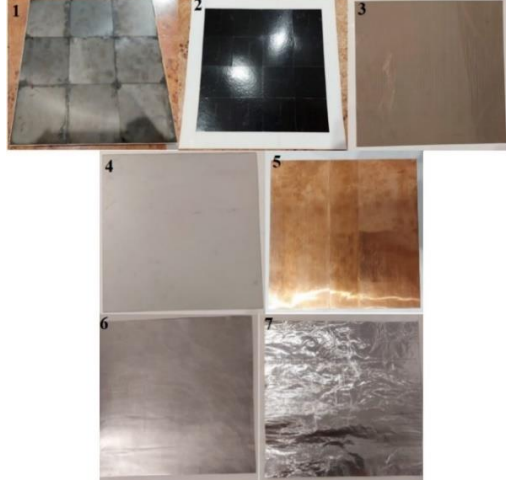
Fig. 5.1. Shields used in the emission coil shielding process

5.2 Shielding Effectiveness (SE)

Shielding is the property of a shield to attenuate the passing of an electric, magnetic or electromagnetic field by: A - Absorption Loss, R - Reflection Loss and M - Multiply Reflection. The Shielding Effectiveness (SE) comprises the sum of the three terms (A, R, M) each representing one of the physical phenomena corresponding to shielding, thus [108]:

$$SE = R + M + A [\text{dB}] \tag{5.1}$$

5.2.1 Near fields and far fields

Relating the distance between the field source and the shield to the wavelength of the field, shielding falls into two categories [108], [116]:
- near-field shielding, where the distance between source and screen (r) versus wavelength (λ) must satisfy the condition $r \ll \lambda/2\pi$,
- the shielding for the plane wave far field shall satisfy the condition $r \gg \lambda/2\pi$.

5.2.2 Reflection shielding
Magnetic field reflection

In the case of the magnetic field, reflection occurs at the output boundary of the wave from the screen, but in order for reflection to be produced, the wave impedance of the medium from which the field comes out (the screen surface) must be greater than the impedance of the medium into which the wave enters from the output of the shield.

Magnetic field reflection losses are [108], [110]:

$$R_m = 14.57 + 10\log\frac{fr^2\sigma_r}{\mu_r} \tag{5.2}$$

where: f - frequency (expressed in Hz), σ_r - relative conductivity of the material, μ_r - relative permeability of the material, r - distance of the source from the screen (expressed in m).

If negative values of R_m are obtained, the term equals 0 and successive reflections M are neglected. If the value of R_m is close to 0, an error occurs based on the non-compliance of the reflection-specific condition $Z_1 \gg Z_2$ [108], [110].

5.2.3 Successive reflection shielding (multiplied)

If the screen thickness t is not bigger compared to the penetration depth δ, then successive reflections and transmission may be important. If (t > δ), the impact of successive reflections is negligible since the absorption losses are significant, if (t < δ) then the attenuation by successive reflections is negative and the shielding effectiveness decreases, the attenuation caused by successive reflection is defined as follows:

$$M = 20 \log\left(1 - e^{-\frac{2t}{\delta}}\right) \text{[dB]} \tag{5.3}$$

5.2.4 Absorption shielding

Absorption screening is a property exclusively of the screen material, it is identical for both the electric or magnetic near field and the far field (plane waves), the absorption is independent of the nature of the field source [114]. The depth limit in the screen material up to which absorption screening occurs is represented by the penetration depth [111], [109], [118], [114]. Absorption attenuation is defined as follows [108]:

$$A = 131 \, t\sqrt{\mu\sigma f} \tag{5.4}$$

where: t - screen thickness (in m).

Following documentation in the literature, the full SE coefficient equation for magnetic fields is:

$$\text{SE} = \text{A} \rightarrow \boxed{131 \, t\sqrt{\mu_r\sigma_r f}} + M \rightarrow \boxed{20 \log\left(1 - e^{-\frac{2t}{\delta}}\right)} + R_m \rightarrow \boxed{14.57 + 10 \log\frac{fr^2\sigma_r}{\mu_r}} \tag{5.5}$$

5.3 Determining the distribusion of magnetic field strength of coils

Three types of coils (planar loop with solid conductor, planar spiral with solid conductor and Litz) of identical diameters and inductances were used to define the magnetic field strength and distribution, which were supplied at a high-frequency alternating voltage (about 6kHz) and tuned to the resonant state by capacitor banks.
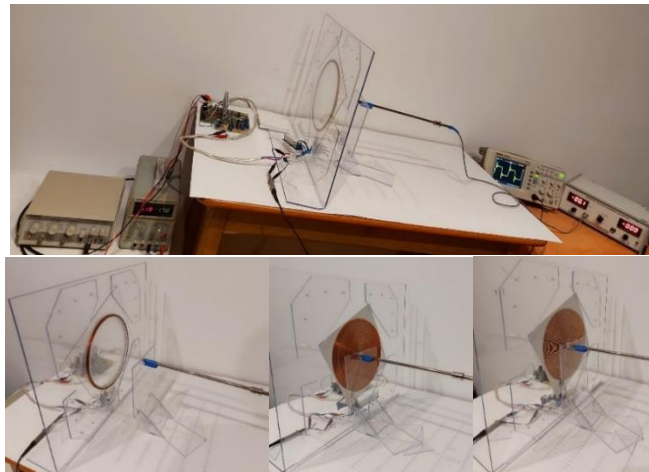
Fig. 5.2. Measurement of magnetic inductance disposition
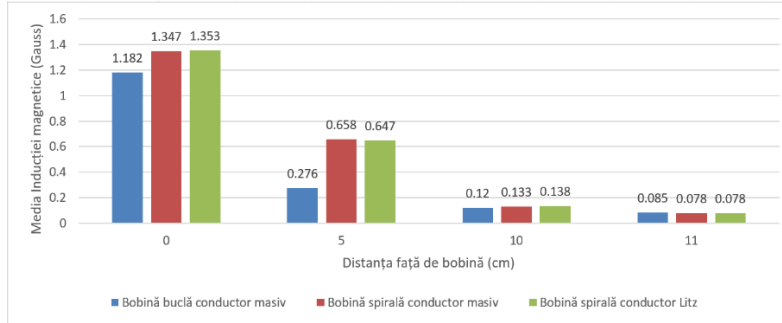
Fig. 5.3. The comparison of average magnetic induction for the three coils

5.4 Constructive shielding solutions

In Table 5.1 the magnetic wave impedance (Z_{W_m}), and for each shielding material the characteristic medium impedance (Z_S) (shield) and penetration depth (δ) were calculated for an operating frequency of f=10.42kHz at a distance between shield and coil of r≈0.6mm (thickness of the coil paper substrate).

Tabel 5.1. Shield impedance (Z_S)), shield-specific penetration depth (δ), magnetic wave impedance (Z_{W_m}) for a frequency f=10.42kHz

f	10.42kHz							
Ecran	1	2	3	4	5	6	7	8
δ	1237.10	45.17	0.00013	0.00064	2.10E-05	0.00064	0.00080	0.00080
Z_S	215690.58	590.69	0.00075	3.76E-05	0.0067	3.75E-05	4.66E-05	4.66E-05
Z_{W_m}	4.93138E-05							

4.4.1 Emission coil shielding

The shielding effectiveness of the transmission coil in a wireless transfer system must contain as high a proportion of the reflection component as possible to increase the magnetic field on the coil extrados. Figure 5.4 shows stages during magnetic induction measurements for different types of shield structures.
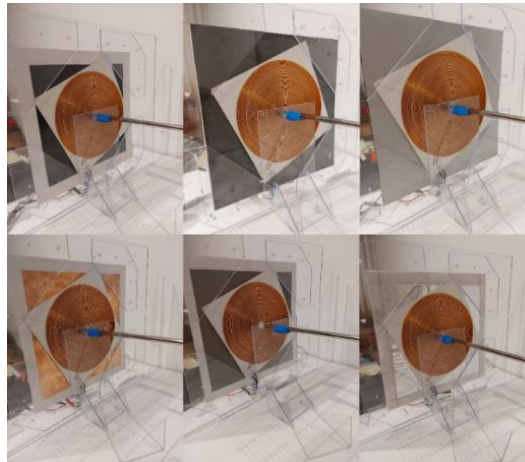
Fig. 5.4. Magnetic induction measurements for shields

Magnetic inductance measurements for each shield were carried out from point to point (13 points), lateral to the center of the coil, at 1 cm intervals. In order to highlight the edge effect of the inductor measurements, intervals of 0.5cm were chosen on the outside area of the coil (9, 9.5, 10, 10.5 - relative to the center of the coil). Measurements were made at the minimum distance from the coil plane ≈0mm, the assembly arrangement being shield-coil-probe measurement, the results are shown in Table 5.2.

Tabel 5.2. The results of measurements and calculations of magnetic induction amplification in dB for each type of shield

| Measured values		B_{A_1}	B_{A_2}														
Shield type		**0**	**A**	**B**	**C**	**D**	**E**	**F**	**G**	**H**	**I**	**J**	**K**	**L**	**M**	**N**	**O**	**P**
	0	3.4	4.1	5.8	5.8	5.7	4.1	4.7	4.3	4.3	4.9	4.5	5	5.1	5.2	7	6.4	5.3
	1	3.2	3.7	5.5	5.5	5.4	4	4.6	3.8	3.9	4.6	4.3	4.8	4.9	4.7	6.4	6	5.1
	2	2.2	2.9	4.6	4.4	4.6	3.2	3.9	3.1	3.1	3.7	3.7	3.8	4.1	3.7	5.2	5	4.1
	3	2	2.3	3.7	3.6	3.5	2.5	3.2	2.5	2.5	2.8	3	3	3.3	2.9	4.1	4	3.2
	4	1.2	1.7	2.7	2.6	2.6	1.9	2.6	1.9	1.9	2.2	2.3	2.2	2.5	2.1	3.2	3.1	2.6
Distance from the centre of coil	5	1.1	1.4	2.1	1.9	1.9	1.5	2	1.4	1.4	1.6	1.8	1.9	2	1.6	2.4	2.3	2.1
	6	0.7	0.9	1.4	1.2	1.3	1	1.6	1	1	1.1	1.2	1.3	1.4	0.9	1.7	1.6	1.4
	7	0.5	0.6	0.9	0.8	0.7	0.6	1	0.6	0.6	0.9	0.7	0.8	1	0.7	1.4	1.1	1.1
	8	0.2	0.1	0.5	0.3	0.3	0.2	0.3	0.1	0.1	0.4	0.2	0.3	0.3	0.2	0.5	0.4	0.5
	9	0	0.2	0.1	0.1	0.3	0.1	0.1	0.3	0	0	0.1	0.1	0.1	0	0.2	0.2	0
	9.5	0.2	0.5	0.6	0.6	0.8	0.4	0.7	0.8	0.5	0.2	0.7	0.5	0.6	0.6	0.9	0.7	0.5
	10	0.4	0.8	1.2	1.2	1.5	0.7	1.2	1.2	0.8	0.7	1	0.8	1	1.1	1.5	1.3	0.8
	10.5	0.4	0.6	1.3	1.4	1.3	1	1.2	1	1	0.8	1.1	0.6	1	1	1.2	1.5	1
Average magnetic field		1.19	1.52	2.33	2.26	2.3	1.63	2.08	1.69	1.62	1.83	1.89	1.93	2.1	1.9	2.74	2.58	2.13
Amplifying (dB)			1.06	2.93	2.78	2.85	1.36	2.43	1.52	1.34	1.88	2.01	2.09	2.46	2.02	**3.62**	3.36	2.52

Tabel 5.3. The inductance variation of coil L1 for each type of shield used and specific amplification in dB

Ecran	A	B	C	D	E	F	G	H	I	J	K	L	M	N	O	P
Amplif. (dB)	1.06	2.93	2.78	2.85	1.36	2.43	1.52	1.34	1.88	2.01	**2.09**	2.46	2.02	**3.62**	3.36	2.52
L	165.4	196.8	196.2	197.5	152.9	180.2	177.8	199.2	192.4	285.8	279.4	266.6	194	278.7	285.1	283.1

5.5 Conclusions

Following the theoretical study and experiments in this chapter we can conclude the following:
- by identifying the magnetic field strength arrangement of the coils, it is clear that loop coils have a lower tolerance to misalignment as compared to planar spiral coils (when using identical transmit and receive coils);
- the varying arrangement of the average magnetic field strengths for different coils suggests that the loop or planar spiral coil type causes a different critical coupling point (critical coupling dependent on coil spacing).

Remark The difference in magnetic field amplification between screen A and E is due to the fact that in screen A, due to the crossing of the Ni layer, losses occur (shielding by absorption) preceded by reflection, whereas in screen E the reflection occurs at the first interaction of the wave with the shield, although the inductance produced by shield E is lower compared to screen A. Another justification is the difference in thickness, screen A has a thickness of 0.8mm (higher losses in the successive-multiplied reflection), while screen E is only 0.2mm thick (lower losses in the successive-multiplied reflection).

6. EFFICIENCY AND POWER
TRANSFERRED WIRELESS - EXPERIMENTAL DETERMINATIONS

Two assumptions on the charging times of drone accumulators are highlighted:

A. Maximum transfer efficiency

B. Maximum power transferred

In order to highlight the effects of load on efficiency and transferred power, optimal load resistances were calculated by setting a range of coupling coefficients k between 0.3-1. Thus at an operating frequency of f=10.42kHz, the optimum load resistances were calculated for coupling air-supported coils, L1 (165.6μH, $R_{L_1} = 0.38\Omega$) with L2 (174.1μH, $R_{L_2} = 0.4\Omega$) and for coupling coils having the shield N attached to the back side of the L1 emission coil with new specific parameters (278. 7μH, $R_{L_1} = 0.38\Omega$) with L2 (174.1μH, $R_{L_2} = 0.4\Omega$). The results are shown in Table 6.1 according to which three values of the load resistances R_L were chosen and used for the following experiments: 31Ω, 11 Ω, 5.6Ω; representing approximately the maximum, minimum and, respectively under-minimum values of the resistances in Table 6.1.

Tabel 6.1. Theoretical determination of the optimum load resistances reported to the coupling coefficient between coils (k)

k	0.3	0.4	0.5	0.6	0.7	0.8	0.9	1
L1 (**165.6**μH, $R_{L_1} = 0.38\Omega$) și L2 (**174.1**μH, $R_{L_2} = 0.4\Omega$)								
$R_{L_{opt}}(\Omega)$	37.7	28.3	22.7	18.9	16.24	14.2	12.6	11.37
M	50.9	67.9	84.9	101.9	118.9	135.8	152.8	169.79
L1 (**278.7**μH, $R_{L_1} = 0.38\Omega$) și L2 (**174.1**μH, $R_{L_2} = 0.4\Omega$)								
$R_{L_{opt}}(\Omega)$	29.1	21.9	17.5	14.6	12.5	11	9.7	8.77
M	66.1	88.1	110.1	132.2	154.2	176.2	198.2	220.27

6.1 Planar spiral coil coupling

Two stages were carried out comprising the coupling behavior of the two coils for a fixed operating frequency and for a variable frequency determined by the maximum received power.

Fig. 6.1. Planar spiral coils - the study of the shield in the emission circuit and the load in the reception circuit

6.2 Planar loop coil coupling

Two stages were carried out which include the coupling behavior of the two coils for a fixed operating frequency and for a variable frequency determined by the maximum received power.
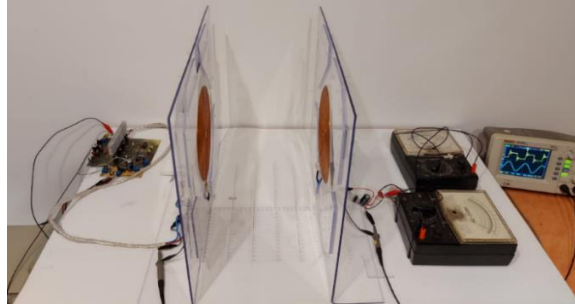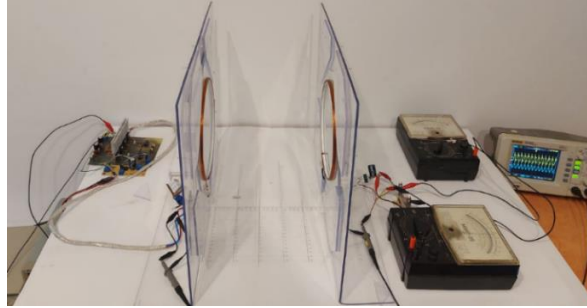
Fig. 6.2. Planar loop coils - the study of the shield in the emission circuit and the load in the reception circuit

6.3 The influence of the shield-emission coil distance on the efficiency and transferred power

In order to identify the effect of the distance between the shield and the emission coil on the magnetic field reflection, with the goal of increasing the transfer efficiency and received power, experiments were performed for the 5.6Ω load used with planar spiral coils, a load that determined the maximum transferred efficiencies and powers in previous experiments (where the distance between the shield and the emission coil was approximately 0). The distances used in the experiments, between the shield and the emission coil are 2mm, 4mm and 8mm, both for the fixed frequency of 10.42kHz and for the frequency determined by the maximum power transferred in the receiving circuit.

I. Influence of the distance between the shield and the emission coil at a fixed operating frequency

II. Influence of the distance between the shield and the emission coil at a variable operating frequency

6.4 Conclusions

Following the results of the experiments carried out in this chapter, the conclusions are presented.

Coupling of planar loop coils

Regarding the study and experiments on wireless power transfer using planar loop coils (both without magnetic support and with the use of N-shield for the emission coil), the respective coils produced much lower results in terms of maximum power transfer and transfer efficiency compared to the experiments using planar loop coils.

Planar spiral coil coupling with respect to the load resistance

In all experiments that define the wireless energy transfer between two planar spiral coils, the maximum values of efficiency and transferred power were obtained for the load resistance 5.6 Ω, which is low compared to the optimum resistances defined for the ideal coupling of k=1, 11.37Ω for the air core coils and 8.77Ω for coils using shield in the emission circuit. For both coil coupling models, the maximum values of efficiency and transferred power were obtained for the load resistance 5.6 Ω. Within the use of load resistors with values of 11 Ω or 31 Ω, exceeding or equal to the 11.37Ω and 8.77Ω resistances specific to the k=1 coupling in Table 6.1, the maximum values of efficiency and transferred power were recorded for increasing coil distances correlated with increasing load resistance.

Planar spiral coil coupling with respect to shield-emission coil distance

For the variable frequency according to maximum received power and 5.6Ω load resistance, a comparison was made between coils coupling with air core and coils coupling using the N-shield for different distances h regarding the emission coil, as shown in Table 6.2.

Tabel 6.2. Comparison between coil coupling in air and coil coupling using
N-shield for different distances

h	f	Distance between coils (cm)	Inverter power supply parameters			Reception parameters with 5.6 ohm load			%	Efficiency Power (2)/ Power (1)	%
			Voltage (1) (V c.c.)	Current (1) (A c.c.)	Power (1) (W)	Voltage (2) (V c.c.)	Current (2) (A c.c.)	Power (2) (W)			
No shield	14.7	0	16	5.1	81.6	13.5	2.45	**33.07**	**0**	0.4053	
	10	0.5	16	3.77	60.32	13	2.25	29.25		0.4849	
	4.5	1	16	2.58	41.28	11	1.9	20.9		**0.5062**	**0**
<1mm	14.7	0	16	5.05	80.8	14.1	2.45	**34.54**	**4.44**	0.4275	
	8.62	0.5	16	3.48	55.68	12.5	2.18	27.25		0.4894	
	6	1	16	2.86	45.76	11.4	2.05	23.37		**0.5107**	**0.88**
2mm	14.3	0	15.6	4.92	76.75	14.1	2.44	**34.40**	**4.02**	0.4482	
	9.2	0.5	16	3.49	55.84	12.25	2.14	26.21		0.4694	
	4.7	1	16	2.53	40.48	10.9	1.93	21.03		**0.5196**	**2.64**
4mm	15	0	16	5.13	82.08	14.25	2.47	**35.19**	**6.41**	0.4288	
	10.8	0.5	16	3.75	60	12.5	2.17	27.12		0.452	
	6.9	1	16	2.79	44.64	11.25	1.95	21.93		0.4914	
	4	1.5	16	2.3	36.8	10.4	1.84	19.13		**0.52**	**2.72**
8mm	14.5	0	16	5.13	82.08	14.25	2.46	**35.05**	**5.98**	0.4270	
	10.6	0.5	16	3.31	52.96	12.5	2.15	26.87		**0.5074**	**0.23**

We can conclude that by positioning the N-shield on the inside of the emission coil there is an increase in efficiency and maximum transferred power compared to the use of the air-supported coupling. At the same time, there is an increase in efficiency and maximum transferred power with an increasing distance between the screen and the coil, with maximum values being recorded at a distance of 4mm.

7. FINAL CONCLUSIONS

For wireless power transfer optimization, theoretical studies found in the technical literature and original experiments were carried out, resulting in an optimal constructive wireless power transfer system version with the following characteristics:

- The emission coil was powered from an H-bridge inverter (supply voltage 16VDC, frequency range ≈2.4-20kHz);

- Emission coil can be used with air support, or for magnetic field increase on the coil extrados, with an N-type shield placed at a distance of 4mm on the coil intrados;

- Mutual coupling M, between planar spiral type emission-reception coils is calculated with equations (3.10), (3.11) resulting in a 22.4% reduction, which has been demonstrated in practice;

- The receiver coil supplies a load (resistive in the experiments) through a rectifier bridge and a voltage stabilizer;

- The self inductance of planar spiral coils is calculated with equation (3.18), the type of solid or Litz conductor does not influence the inductance at low frequencies as long as the effective diameters of the conductors are identical;

- Planar loop coils offer much lower efficiency and transferred power rates than planar spiral coils, therefore they are not recommended in the field of wireless power transfer;

- Optimum load in the reception is defined by the quality coefficients of the systems.

In order to wirelessly supply a real load of 31Ω (theoretically calculated as 33.59) with a power of 30W ,at a distance of 1cm, a magnetic coupling of two coils L1(165.6μH) and L2 (174.1μH) with a parallel capacitor for each coil C=1.40μF, will be used, with a frequency of 15.6kHz; a total efficiency of 40% being obtained. Maximum efficiencies of 43% were obtained for a 1.5cm distance with 25.76W received and for a 2cm distance with 20W received. Each coupling coefficient between two coils corresponds to an optimal resistance value, if the same distance between coils (1cm) is maintained but a lower load resistance (5.6Ω) is used, the transfer efficiency will increase but the transferred power will decrease.

Therefore, for the same coil configuration but for a 5.6Ω load at ≈0cm distance a power of 33.7w was received (40% efficiency) and at 1cm distance a power of 20.0W was received (efficiency 50%); introducing the N screen, at ≈0cm distance a power of 35.19W was received (efficiency 42.8%), at 1cm distance a power of 21.93W was received (efficiency 49.1%) and at 1.5cm distance a power of 19.13W was received (efficiency 52%).

Thus, in the case of using sandwich shields on the extrados of the emission coil for magnetic field reflection, there was a 6.41% increase in the maximum power transferred compared to the experiment using air core for the emission coils. An important aspect is the distance between the screen and the emission coil which should be about 2% of the coil diameter.

It should be noted that the efficiencies are global and include losses through DC-AC conversion (transmit inverter) and AC-DC (reset, receive stabilization).

8. ORIGINAL CONTRIBUTIONS

The main original contributions that the author brings to the realization of this research thesis are presented in the following steps:

- the first stage consisted in carrying out an analysis of the current state of wireless powering of various devices, a stage that was completed with a short introduction experiment necessary to identify and understand the phenomena and limitations of wireless power transfer;

- before the simulations and experiments, the complete mathematical model of wireless power transfer was developed by demonstrating and mathematically validating the phenomena of reflected impedance, maximum power transfer, and maximum efficiency and calculating the optimal load for maximum efficiency as a function of the quality coefficients of the emission and reception systems;

- the self and mutual inductances of the planar loop and planar spiral coils chosen for the experiments were calculated using Matlab ; limitations in the use of literature calculation equations were identified for the inductances of planar spiral coils; for planar loop coils, the literature equations were modified to match the calculated and measured inductance values; for both types of coils, precise calculation equations were established and validated with real measurements;

- three types of inverters have been designed and simulated in the Matlab environment and the H-bridge inverter has been completely built and optimized for use in experiments;

- clear equations were drawn from the specific literature to define the effectiveness of the shields, several shield designs were tested to increase the proportion of reflection shielding and an optimal shield model was identified in the materials under testing;

- final experiments were carried out on efficiency and maximum transferred power, with clear correspondences between the distance between coils determining the critical coupling, the maximum efficiency versus the load resistance used in reception;

- the influence of the distance between the shield and the emission coil on efficiency, transferred power and reflection shielding was determined experimentally and theoretically.

Therefore, the personal contribution of this doctoral thesis is represented by the whole process of realization of the wireless power transfer system to a load, consisting of design, simulation, modeling and construction of coil-inverter-shield, and experimentation.

This work contains the theoretical and practical fundamentals necessary to realize a wireless transfer system for a desired load and power, moreover, new scientific aspects, identified from the research were carried out in this thesis, which improve the efficiency and transferred power compared to a simple, non-optimized wireless system are presented.

9. PERSPECTIVES FOR FURTHER RESEARCH

Based on the theoretical and practical results of the research in this doctoral thesis, new directions for further scientific research on wireless power transfer are highlighted as follows:

The study of wireless energy transfer as an effect of different variants of serial, parallel or mixed connection types of emission and reception circuits.

Development of an automatic calculation program of the characteristics of a wireless transfer system for a received power, given a certain load and distance, both in terms of electrical parameters and physical characteristics of the coils used.

The wireless transfer design for higher resonant frequencies above 20kHz in terms of propagation in different environments.

Introduction of Class E inverters in wireless transfer systems for experiments.

Use of shield concepts for electromagnetic field reflection using new materials, shapes or sequences to increase the efficiency and power transferred in a wireless system.

10. BIBLIOGRAPHY

10.1 Bibliography Cap. 1

[1]. https://www.britannica.com - accesed at 20.10.2022

[2]. https://www.invent.org/inductees/oliver-joseph-lodge - accesed at 20.10.2022

[3]. https://www.istro-romanian.net/articles/art990111.html - accesed at 20.10.2022

[4]. Surendra Pal, Sir Jagdish Chandra Bose, James Clerk Maxwell and there on….., IEEE India Info. Vol. 14 No. 2 Apr - Jun 2019

[5]. https://monoskop.org/Jozef_Murga%C5%A1 - accesed at 20.10.2022

[6]. https://www.radioromaniacultural.ro/ - accesed at 20.10.2022

[7]. https://www.nobelprize.org/prizes/physics/1909/marconi/biographical/ - accesed at 20.10.2022

[8]. Mihai Iordache, Marilena Stanculescu, Lavinia Bobaru, Dragos Niculae, Sorin Deleanu, Victor Bucata, Sisteme de transfer wireless al energiei electromagnetice, Universitatea Politehnica Bucuresti, ISBN: 978-606-25-0623-0

[9]. https://www.imperial.ac.uk/news/191606/testing-waters-challenge-wireless-power-lab/ - accesed at 20.10.2022

[10]. https://www.wartsila.com/ - accesed at 24.07.2022

[11]. https://www.media.volvocars.com/global/en-gb/media/pressreleases/295720/volvo-cars-tests-new-wireless-charging-technology - accesed at 24.07.2022

[12].https://www.moveelectric.com/e-cars/volvo-test-new-wireless-charging-technology - accesed at 24.07.2022

[13]. Bo Zhang, Richard B. Carlson, John G. Smart, Eric J. Dufek, and Boryann Liaw, Challenges of Future High Power Wireless Power Transfer for Light-Duty Electric Vehicles----Technology and Risk Management, Clean Energy and Transportation Division, Idaho National Laboratory, 2525 N. Fremont Ave., Idaho Falls, ID 83415, USA, October 2019

[14]. Richard M. Dickinson, Wireless power transmission technology state of the art the first Bill Brown lecture, Acta Astronautica, Volume 53, Issues 4–10, August–November 2003, Pages 561-570 https://doi.org/10.1016/S0094-5765(03)80017-6

[15]. **Vlad Mocanu**, Petrica Popov and Vasile Dobref, Charging floating bases for marine unmanned aerial droneScientific Bulletin of Naval Academy, Vol. XXIII 2020, pg.116-121, doi: 10.21279/1454-864X-20-I1-015

[16]. José Antonio Luceño-Sánchez, Ana María Díez-Pascual, Rafael Peña Capilla, Materials for Photovoltaics: State of Art and Recent Developments, International Journal of Molecular Sciences, 23 February 2019

[17]. Nicolae-Silviu POPA , Mihai-Octavian POPESCU, Vlad **MOCANU**, Producing Electricity with Photovoltaic Panels in Motion and Discharging Li-ion Batteries, THE 13th INTERNATIONAL SYMPOSIUM ON ADVANCED TOPICS IN ELECTRICAL ENGINEERING March 23-25, 2023 Bucharest, Romania

[18]. Photovoltaics report, Prepared by Fraunhofer Institute for Solar Energy Systems, ISE with support of PSE GmbH Freiburg, 14 November 2019

[19]. R.W. Miles, K.M. Hynes, I. Forbes, Photovoltaic solar cells: An overview of state-of-the-art cell development and environmental issue, Progress in Crystal Growth and Characterization of Materials, Volume 51, Issues 1–3, 2005, Pages 1-42

[20]. https://www.climatestotravel.com/climate/romania#coast - accesat la 24.07.2022

[21]. X. Wei, Z. Wang, and H. Dai, A Critical Review of Wireless Power Transfer via Strongly Coupled Magnetic Resonances, Energies, vol. 7, no. 7, pp. 4316-4341, July 2014, doi:10.3390/en7074316

[22]. N. Shinohara, The Wireless Power Transmission: Inductive Coupling, Radio Wave, and Resonance Coupling, vol. 1, no. 3, pp. 337-346, Dec.2012, https://doi.org/10.1002/wene.43

[23]. N. Shinohara, Power Without Wires, IEEE Microwave Magazine, vol.12, no. 7, pp. S64-S73, Dec. 2011, DOI: 10.1109/MMM.2011.942732

[24]. **MOCANU Vlad**, POPOV Petrică, DOBREF Vasile, DELIU Florenţiu, CRISTEA Ovidiu, Improving the inductive wireless power transfer for marine aerial drones charging, ELECTROTEHNICĂ, ELECTRONICĂ, AUTOMATICĂ (EEA), 69 (2021), nr. 3, pp. 55-63 DOI:10.46904/eea.21.69.3.1108007

[25]. Jin Xu ,Yuhui Xu, Qian Zhang, Calculation and analysis of optimal design for wireless power transfer, Computers and Electrical Engineering, vol.80, December 2019, 106470, https://doi.org/10.1016/j.compeleceng.2019.106470

[26]. Rikard Vinge, Wireless Energy Transfer by Resonant Inductive Coupling, Master of Science Thesis, Department of Signals and systems CHALMERS UNIVERSITY OF TECHNOLOGY Göteborg, Sweden 2015

[27]. Omar Abdel-Rahim, Wireless Power Transfer Report, Electrical and Electronic Eng. Dept., Utsunomiya University, June 2015

[28]. Klaus Finkenzeller, FUNDAMENTALS AND APPLICATIONS IN CONTACTLESS SMART CARDS, RADIO FREQUENCY IDENTIFICATION AND NEAR-FIELD COMMUNICATION, pp. 69/111, Giesecke & Devrient GmbH, Munich, Germany, John Wiley & Sons, Ltd. Publication, THIRD EDITION, 2010

[29]. Y. Wanderoild, A. Morel, G. Pillonnet, D. Bergogne, Hubert Razik, Maximizing Wireless Power Transfert with Single-Turn Coreless Coupled Coils, IEEE International Symposium on Circuits and Systems (ISCAS), 2018

[30]. J. D. Jackson, Classical Electrodynamics. Wiley, New York, 3rd. edition, 1999

[31]. Huseyin U. Aydogmus, Hakan P. Partal, Modeling and Simulation of Multilayer Rectangular Coils for Wireless Power Transfer Applications, International Applied Computational Electromagnetics Society (ACES) Symposium, Miami, 2019

[32]. Jordi-Roger Riba, Analysis of formulas to calculate the AC resistance of different conductors' configurations, Escola d'Enginyeria d'Igualada, Universitat Politècnica de Catalunya, Pla de la Massa 8, 08700 Igualada, Spain

10.2 Bibliography Cap. 2

[33]. Minh T. Nguyen, Cuong V. Nguyen, Linh H. Truong, Anh M. Le, Toan V. Quyen,Antonino Masaracchia, Keith A. Teague, Electromagnetic Field Based WPT Technologies for UAVs: A Comprehensive Survey, Electronics 2020, Electrical and Autonomous Vehicles), 9(3), 461, https://doi.org/10.3390/electronics9030461

[34]. Sotir Alexandru, Teoria campului electromagnetic, Note de curs IFR, Constanța: Editura Academiei Navale „Mircea cel Bătrân", 2015

[35]. *Radu Ianculescu, Manualul radioamatorului începător, Editura Tehnică Bucureşti, 1989*

[36]. SAMUEL *J. LING, JEFF SANNY, WILLIAM MOEBS, University physics volume 2, OpenStax Rice University, 6100 Main Street MS-375, Houston, Texas 770052016, 2021*

[37]. Lucia Dumitriu, Cătălin Dumitriu, BAZELE ELECTROENERGETICII, BUCUREŞTI, 2004

[38]. A. Moraru, Bazele electrotehnicii – Teoria câmpului electromagnetic, Editura Matrix-Rom, București, 2002

[39]. Constantinescu Stelian, Radiotehnica teoretică și practică vol. 1, Editura Militară a Ministerului Forțelor Armate ale R.P.R, București, 1959

[40]. Edmond Nicolau, Radiația și propagarea undelor electromagnetice, Editura Academiei Republicii socialiste Romania, București 1989.

[41]. Johnson I. Agbinya, Wireless Power Transfer 2nd edition, River Publishers Series in Communications, 2016

[42]. Partha Sarathi Subudhi, Krithiga S, Wireless Power Transfer Topologies used for Static and Dynamic Charging of EV Battery: A Review, International Journal of Emerging Electric Power Systems. 2020, https://doi.org/10.1515/ijeeps-2019-0151

[43]. Woo-Seok Lee, Jin-Hak Kim, Shin-Young Cho, Il-Oun Lee 1, An Improved Wireless Battery Charging System, Energies 2018, 11, 791; doi:10.3390/en11040791

[44]. Yoshio Mita, Naoyuki Sakamoto, Naoto Usami, Antoine Frappé, Akio Higo, Bruno Stefanelli, Hidehisa Shiomi, Julien Bourgeois, Andreas Kaiser, Microscale ultrahigh-frequency resonant wireless powering for capacitive and resistive MEMS actuators, Sensors and Actuators A: Physical Volume 275, 1 June 2018, Pages 75-87, https://doi.org/10.1016/j.sna.2018.03.020

[45]. Lucia Dumitriu, Mihai Iordache, Dragos Nicolae, Witricity, Universitatea Politehnica din Bucuresti Facultatea de Energetica Catedra de Electroenergetica, Bucuresti 2011

[46]. Nicolau Mircea, Chiculescu Iosif, Bazele teoretice ale radiotehnicii, vol. I, Academia militară generală, aprilie 1967

[47]. **V. MOCANU**, V. DOBREF, F. DELIU, O. CRISTEA, P. POPOV, M. TÂRHOACĂ, Design of series-series oscillating circuits used in wireless transmission of electricity for battery charging, Scientific Bulletin of Naval Academy, Vol. XXIV 2021, pg.23-32, doi:10.21279/1454-864X-21-I2-002

[48]. Michael W. Baker, Rahul Sarpeshkar, Feedback Analysis and Design of RF Power Links for Low-Power Bionic Systems, IEEE TRANSACTIONS ON BIOMEDICAL CIRCUITS AND SYSTEMS, VOL. 1, NO. 1, MARCH 2007, DOI: 10.1109/TBCAS.2007.893180

[49]. Sushree S. Biswal, Durga P. Kar, Satyanarayan Bhuyan, Parameter Trade-off between Electric Load, Quality Factor and Coupling Coefficient for Performance Enrichment of Wireless Power Transfer System, Progress In Electromagnetics Research M, Vol. 91, 49–58, 2020, DOI:10.2528/PIERM20010902

[50]. Mehdi Kiani, Maysam Ghovanloo, The Circuit Theory Behind Coupled-Mode Magnetic Resonance-Based Wireless Power Transmission, IEEE TRANSACTIONS ON CIRCUITS AND SYSTEMS-I: REGULAR PAPERS, VOL. 59, NO. 9, SEPTEMBER 2012, DOI: 10.1109/TCSI.2011.2180446

[51]. Sebastian Toader Arădoaei, Adrian Adăscăliței, Teoria circuitelor electrice I, pp.: 61, 218-220, Editura Pim, 2019

[52]. Klaus Finkenzeller, RFID HANDBOOK FUNDAMENTALS AND APPLICATIONS IN CONTACTLESS SMART CARDS, RADIO FREQUENCY IDENTIFICATION AND NEAR-FIELD COMMUNICATION, THIRD EDITION, pp. 85-96, Ed. John Wiley & Sons, Ltd., 2010

[53]. L H Liang, Z Z Li , Y J Hou, H Zeng, Z K Yue, S Cui, Study on frequency characteristics of wireless power transmission system based on magnetic coupling resonance, IOP Conf. Series: Earth and Environmental Science 93, (2017), doi:10.1088/1755-1315/93/1/012063

[54]. Emil Cazacu, Bazele electrotehnicii I și II-Teoria circuitelor electrice liniare, pp.:34-35, 44-47, 141, 2012

[55]. THOMAS H. LEE - Stanford University, THE DESIGN OF CMOS RADIO-FREQUENCY INTEGRATED CIRCUITS - SECOND EDITION, CAMBRIDGE UNIVERSITY PRESS, 2004, ISBN 978-0-521-83539-8

[56]. CONSTANTIN STRÎMBU, Semnale şi Circuite Electronice – Circuite de prelucrare a semnalelor, Editura Academiei Forţelor Aeriene "Henri Coandă", 2010

[57]. Adrian A. ADĂSCĂLIŢEI, TEORIA CIRCUITELOR ELECTRICE, Editura PERFORMANTICA Institutul Naţional de Inventică, Iaşi, 2015

10.3 Bibliography Cap. 3

[58]. MARIAN PEARSICĂ, ELECTROTEHNICĂ, Editura Academia Forţelor Aeriene „Henri Coandă", 2004

[59]. Nicolae Badea, Ion Voncică, Teorie câmpului electromagnetic, Editura Fundaţiei Universitare „Dunărea de Jos" Galaţi, 2003

[60]. Xu Liu, Chenyang Xia, Xibo Yuan, Study of the Circular Flat Spiral Coil Structure Effect on Wireless Power Transfer System Performance, Energies 2018, 11, 2875; doi:10.3390/en11112875

[61]. Alan Payne, SKIN EFFECT, PROXIMITY EFFECT AND THE RESISTANCE OF CIRCULAR AND RECTANGULAR CONDUCTORS, May 2021

[72]. Alexandru SOTIR, Bazele electrotehnicii. Teoria circuitelor electrice. Teoria câmpului electromagnetic, Ediţia a-V-a revizuită, Editura Academiei Navale „Mircea cel Bîtrân", 2014

[63]. Sergiu IVAS, Teoria macroscopică a câmpului electromagnetic, Editura Fundaţiei Universitare „Dunărea de Jos" Galaţi, 2003

[64]. https://www.tme.eu/Document/74d729cd343ae433e6f31d797dd3fab1/W210_pl.pdf (https://www.tme.eu/ro/)

[65]. Jinwook Kim, Approximate Closed-Form Formula for Calculating Ohmic Resistance in Coils of Parallel Round Wires with Unequal Pitches, IEEE TRANSACTIONS ON INDUSTRIAL ELECTRONICS, 2014, DOI 10.1109/TIE.2014.2370943

[66]. Vesa Väisänen, Jani Hiltunen, Janne Nerg, Pertti Silventoinen, AC Resistance Calculation Methods and Practical Design Considerations When Using Litz Wire, IECON 2013 - 39th Annual Conference of the IEEE Industrial Electronics Society, January 2014, DOI: 10.1109/IECON.2013.6699164

[67]. New England Wire Technologies, LITZ & WINDING WIRES, 2005

[68]. https://www.tme.eu/ro/katalog/sarma-bobinata_100610/?mapped_params=662%3A1451240%3B (https://www.tme.eu/ro/)

[69]. Fernandez, C.; Garcia O.; Prieto R.; Cobos J.A.; Gabriels S.; Borght, G. Van Der Borght, Design Issues of a Core-less Transformer for a Contact-less Application, Dallas TX USA, APEC. Seventeenth Annual IEEE Applied Power Electronics Conference and Exposition, doi:10.1109/APEC.2002.989268, 07 August 2002

[70]. James Lawson, High Frequency Electromagnetic Links for Wireless Power Transfer, Thesis submitted in partial fulfilment of the requirements for the degree of Doctor of Philosophy of Imperial College London and the Diploma of Imperial College, London, SW7 2AZ, United Kingdom, January 2017

[71]. https://www.elektrisola.com/en/Litz-Wire/Info

[72]. THOMAS H. LEE - Stanford University, THE DESIGN OF CMOS RADIO-FREQUENCY INTEGRATED CIRCUITS - SECOND EDITION, CAMBRIDGE UNIVERSITY PRESS, 2004, ISBN 978-0-521-83539-8

[73]. Nicolau Mircea, Chiculescu Iosif, Bazele teoretice ale radiotehnicii, vol. I, Editat în Academia Militară Generală, aprilie 1967

[74]. Vasile Ciobanița, Iosif Lingvay, Ilie Matra, Alexandru Marculescu, Ilie Mihaescu, Adrian Nicolae, George D. Oprescu, George Pintilie, Imre Szatmary, Mihail Silisteanu, Vasile Vacaru, RADIORECEPȚIA, Editura albatros Bcururesti, 1982

[75]. Rithvik Reddy Adapap; Syed Sarfaraz Nawaz; Dola Gobinda Padhan, Analytical Study of Magnetic Flux Density for Circular Spiral and Square Spiral Coils, DOI: 10.1109/SeFet48154.2021.9375764, 2021

[76]. C. M. Zierhofer, E. S. Hochmair, Geometric Approach for Coupling Enhance t of Magnetically Coupled Coils, IEEE TRANSACTIONS ON BIOMEDICAL ENGINEERING, VOL. 43, NO. 7, JULY 1996, DOI: 10.1109/10.503178

[77]. Rikard Vinge, Wireless Energy Transfer by Resonant Inductive Coupling, Master of Science Thesis, Department of Signals and systems, CHALMERS UNIVERSITY OF TECHNOLOGY, Göteborg, Sweden 2015

[78]. Vlad **MOCANU**, Mihai Octavian POPESCU, Vasile DOBREF, Nicolae-Silviu POPA, OPTIMIZATION OF COIL INDUCTANCE EQUATIONS USED IN WIRELESS POWER TRANSFER FOR DRONE CHARGING, U.P.B. Sci. Bull., Series C Electrical Engineering and Computer Science, 2023, ISSN 2286-3559

[79]. Alicia Triviño-Cabrera, José M. González-González, José A. Aguado, Wireless Power Transfer for Electric Vehicles: Foundations and Design Approach, Springer Nature Switzerland AG 2020, https://doi.org/10.1007/978-3-030-26706-3, Power Systems ISBN 978-3-030-26705-6

[80]. https://www.deepfriedneon.com/tesla_f_calcspiral.html

[81]. *Suresh Atluri, Maysam Ghovanloo*, Design of a Wideband Power-Efficient Inductive Wireless Link for Implantable Biomedical Devices Using Multiple Carriers, Conference Proceedings. 2nd International IEEE EMBS Conference on Neural Engineering, 2005

[82]. *Mare T. Thompson*, Inductance Calculation Techniques Part II: Approximations and Methods, Power Control and Intelligent Motion, December 1999

[83]. *Thuc Phi Duong, Jong-Wook Lee*, A Dynamically Adaptable Impedance-Matching System for Midrange Wireless Power Transfer with Misalignment, *Energies* 2015, *8*(8), 7593-7617.

[84]. *Zifan Dong; Xiaoming Li; Sheng Liu; Ziwei Xu; Lin Yang*, A Novel All-Direction Antimisalignment Wireless Power Transfer System Designed by Truncated Region Eigenfunction Expansion Method, IEEE Transactions on Power Electronics, vol. 36, Issue: 11, November 2021

10.4 Bibliography Cap. 4

[85]. Zbigniew Kaczmarczyk, A high-efficiency Class E inverter–computer model, laboratory measurements and SPICE simulation, BULLETIN OF THE POLISH ACADEMY OF SCIENCESTECHNICAL SCIENCES, Vol. 55, No. 4, 2007

[86]. Woo-Seok Lee, Jin-Hak Kim, Shin-Young Cho, Il-Oun Lee, An Improved Wireless Battery Charging System, Energies 2018, 11(4), 791, 2018, https://doi.org/10.3390/en11040791

[87]. Sang-Won Lee, Yoon-Geol Choi, Jung-Ha Kim, Bongkoo Kang,Wireless Battery Charging Circuit Using Load Estimation Without Wireless Communication, November 2019, Energies 12(23):4489, DOI:10.3390/en12234489

[88]. **Mocanu V**, Dobref V, Popov P, Aspects regarding the use of passive filters for harmonic mitigation in power rectifiers, Scientific Bulletin "Mircea cel Batran" Naval Academy; Constanta Vol. 23, Iss. 2, (2020): 1-12

[89]. Abdelmajid Sarraj, Wael Dghais, S. Barmada, M. Tucci, M. Raugi, Harmonic distortion considerations for an integrated WPT-PLC system, Wireless Power Transfer, Volume 7, Issue 1, March 2020, pp. 33 – 41, DOI: https://doi.org/10.1017/wpt.2020.4

[90]. Katsuhiro Hata, Takehiro Imura, Yoichi Hori, Analysis and Experiment on Harmonic Current Distortion in Wireless Power Transfer System Using a Diode Rectifier, IECON2015-Yokohama, November 9-12, 2015

[91]. Seyit Ahmet Sis, Hakan Akca, Maximizing the efficiency of wireless power transfer systems with an optimal duty cycle operation, AEU - International Journal of Electronics and Communications, March 2020, DOI:10.1016/j.aeue.2020.153081

[92]. **Mocanu Vlad**, Dobref Vasile, Deliu Florențiu, Popa Nicolae-Silviu, A multidimensional comparative analysis of inverters used in wireless power transfer, 2022 8th International Conference on Energy Efficiency and Agricultural Engineering (EE&AE), doi: 10.1109/EEAE53789.2022.9831412

[93]. **Mocanu Vlad**, Popescu Mihai Octavian, Dobref Vasile, Popa Nicolae-Silviu, Design and Construction of an H-bridge Inverter used in Wireless Power Transfer, THE 13th INTERNATIONAL SYMPOSIUM ON ADVANCED TOPICS IN ELECTRICAL ENGINEERING March 23-25, 2023 Bucharest, Romania

[94]. Chris Cockrill - Texas Instruments, Understanding Schmitt Triggers, Application Report SCEA046–September 2011, www.ti.com - accesed at 20.10.2022

[95]. CDx4HC14 Hex Inverters with Schmitt-Trigger Inputs, SCHS129G JANUARY 1998 – REVISED MAY 2021, www.ti.com - accesed at 10.10.2022

[96]. https://soldered.com/learn/hum-the-simple-h-bridge/

[97]. Infineon Technologies, Data Sheet No. PD60026 revS - HIGH AND LOW SIDE DRIVER www.irf.com - accesed at 01.03.2022

[98]. www.engineersgarage.com (Testing IR2110 Gate Driver IC) - accesed at 25.10.2022

[99]. Data Sheet No. PD60147K, IR2110/IR2113, https://manualzz.com

[100]. https://electel.blogspot.com/2016/01/using-high-low-side-driver-ir2110.html

[101]. https://electronics.stackexchange.com/questions/18423/bootstrap-capacitor-selection-with-ir2110-3

[102]. Mamadou Diallo - Texas Instruments High Power Drivers, Bootstrap Circuitry Selection for Half-Bridge Configurations Application Report SLUA887–August 2018, www.ti.com - accesed at 20.4.2022

10.5 Bibliography Cap. 5

[103]. https://ro.farnell.com/wurth-elektronik/354004/ferrite-sheet-sheilding-square/dp/2420804 - accesed at 01.11.2022

[104]. https://ro.farnell.com/wurth-elektronik/354004/ferrite-sheet-sheilding-square/dp/2420804 - accesed at 01.11.2022

[105]. https://ro.farnell.com/3m/cn-3190-sheet/emi-shielding-sheet/dp/2309124 - accesed at 01.11.2022

[106]. http://www.physics.pub.ro/Cursuri/Mihaela_Ghelmez_-_Optica.pdf - accesed at 01.11.2022

[107]. https://www.kemet.com/en/us/technical-resources/how-to-manage-loss-efficiently-with-ferrite-tiles-in-wireless-power-transfer.html - accesed at 01.11.2022

[108]. Henry W. Ott, Henry Ott Consultants, Electromagnetic Compatibility Engineering, Published by John Wiley & Sons, Inc., Hoboken, New Jersey, 2009

[109]. Gheorghe Săndălău, PROTECȚIA LA PERTURBAȚII ÎN ELECTRONICA APLICATĂ RADIO ȘI TV, Editura Militară București, 1990

[110]. CLAYTON R. PAUL, Introduction to Electromagnetic Compatibility, Published by John Wiley & Sons, Inc., Hoboken, New Jersey, 2006

[111]. Stanislav Kovar, Jan Valouch, Hana Urbancokova, Calculation of Shielding Effectiveness of Materials for Security Devices, MATEC Web of Conferences 125, 02036 (2017), CSCC 2017, DOI: 10.1051/matecconf/201712502036

[112]. Simu Călin, Mârza Eugen-Antene radio-TV, Ed. Orizonturi Universitare, Timișoara, 2001

[113]. Matthew Schwartz, "Refraction and Reflection," Lecture note. [Online]. Available: https://scholar.harvard.edu/files/schwartz/files/lecture15-refraction.pdf - accesed at 30.10.2022

[114]. SALVATORE CELOZZI RODOLFO ARANEO GIAMPIERO LOVAT, Electromagnetic Shielding, Electrical Engineering Department ''La Sapienza'' University Rome, Italy, A JOHN WILEY & SONS, INC., PUBLICATION, 2008, ISBN 978-0-470-05536-6

[115]. https://www.britannica.com/science/refractive-index - accesed at 01.11.2022

[116]. https://interferencetechnology.com/shielding-effectiveness-near-field-far-field/ - accesed at 12.11.2022

[117]. George M. Kunkel, Shielding of Electromagnetic Waves, ISBN 978-3-030-19237-2, https://doi.org/10.1007/978-3-030-19238-9, Springer Nature Switzerland AG 2020

[118]. Xingcun Colin Tong, Advanced Materials and Design for Electromagnetic Interference Shielding, © 2009 by Taylor & Francis Group, LLC, ISBN 13: 978-1-4200-7358-4

[119]. Win-Jet Luo, C. Bambang Dwi Kuncoro, Pratikto Sunkar, Yean-Der Kuan, Single-Layer Transmitter Array Coil Pattern Evaluation toward a Uniform Vertical Magnetic Field Distribution, Energies 2019,12, 4157; doi:10.3390/en12214157

[120]. https://www.thoughtco.com/table-of-electrical-resistivity-conductivity-608499 - accesed at 15.01.2023

[121]. D. Ravinder, K. Latha, Electrical conductivity of Mn–Zn ferrites, Journal of Applied Physics 75, 6118 (1994); doi: 10.1063/1.355479

[122]. https://www.engineeringtoolbox.com/ - Electrical Conductivity - Elements and other Materials - accesed at 16.01.2023

[123]. https://www.electronics-tutorials.ws/ - Decibels - accesed at 20.01.2023
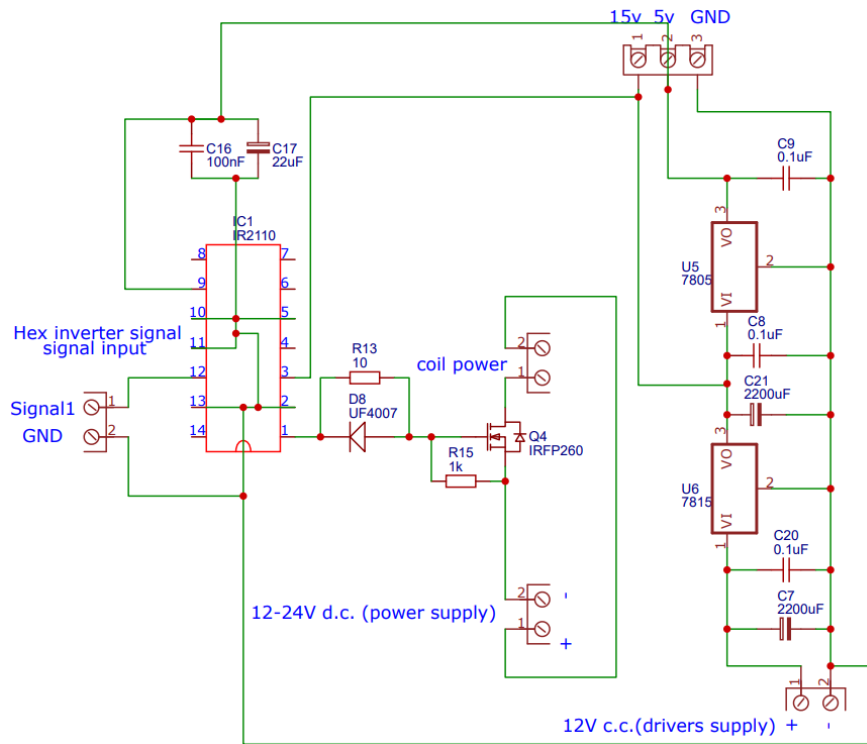
11. APPENDIX

Anexa 1. Complete H-bridge inverter diagram used in the experiment
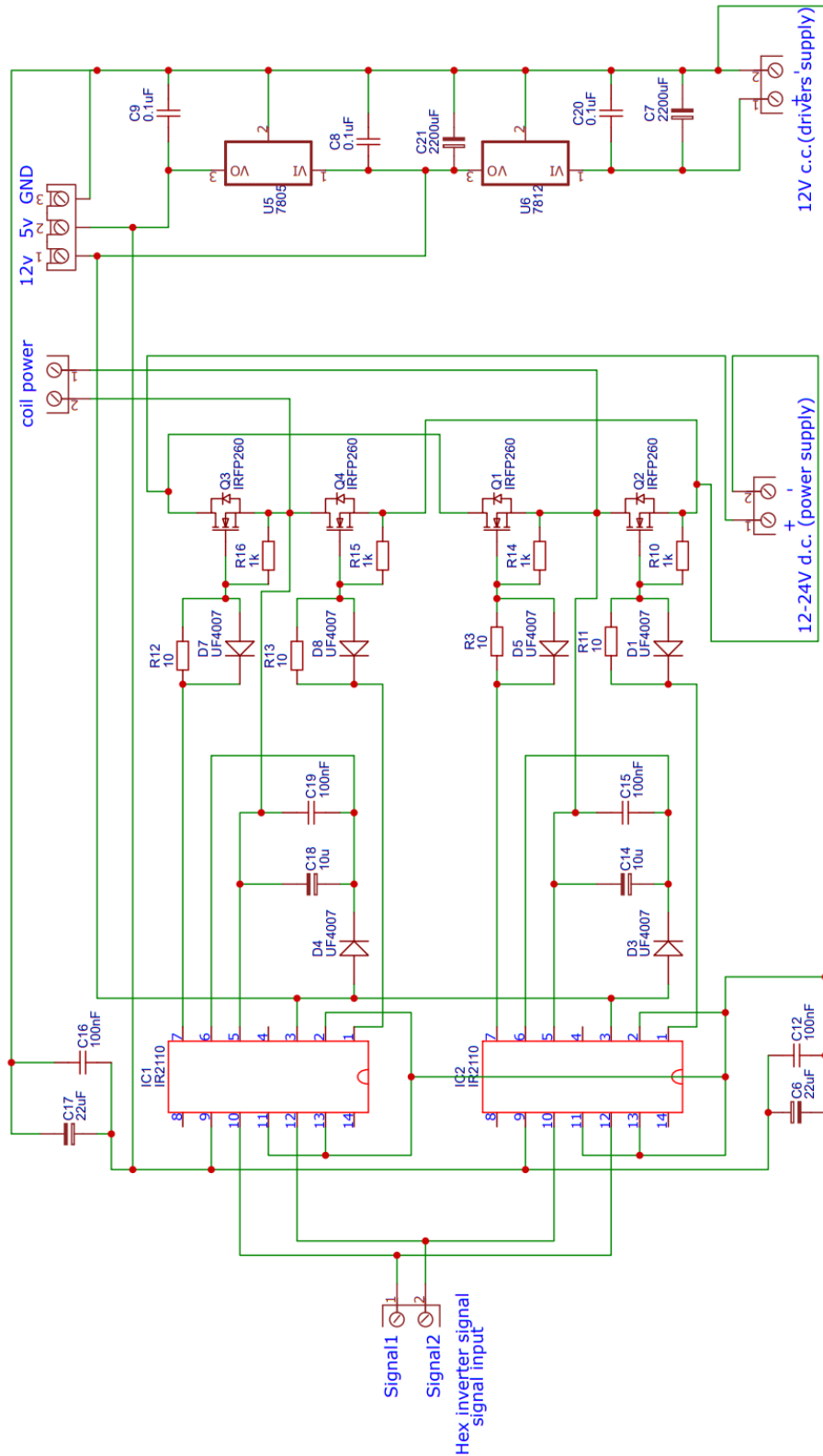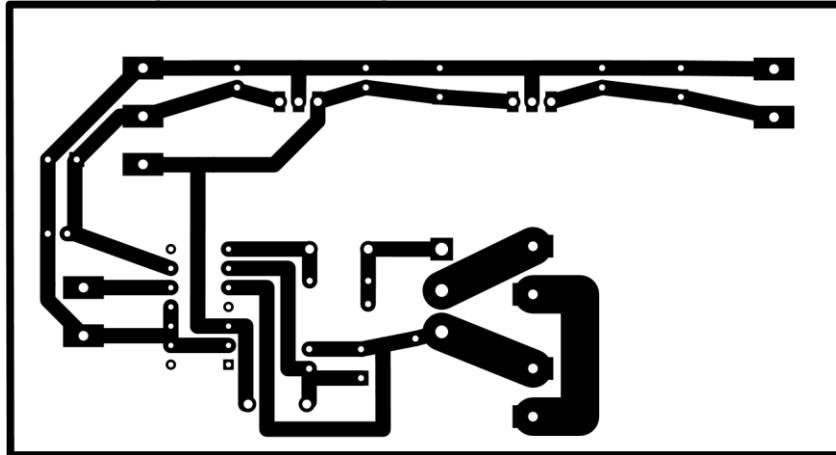
Anexa 2. Class E (High side) inverter diagram
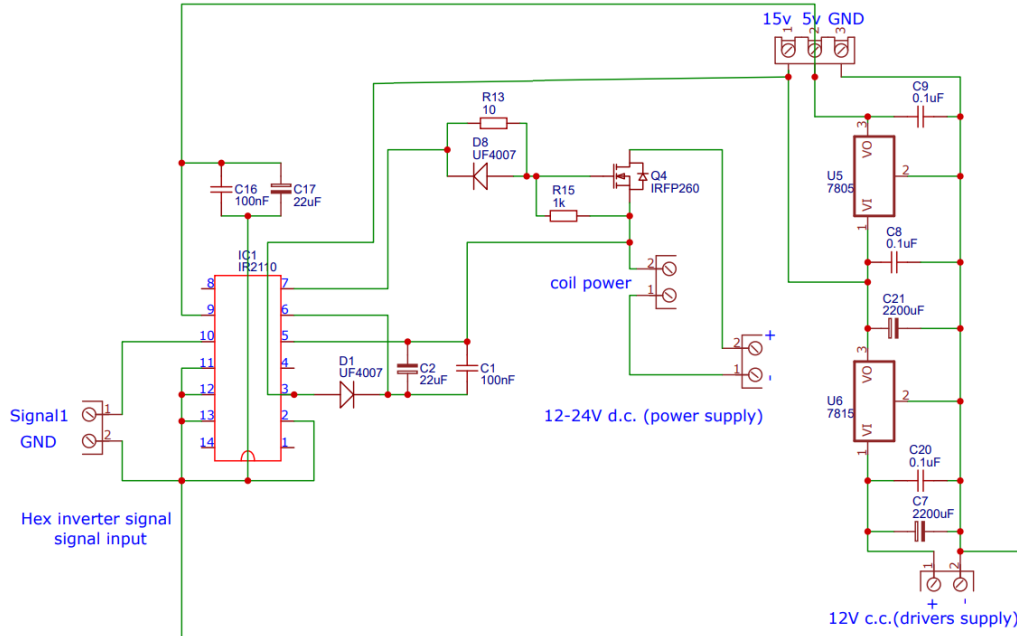
Anexa 3. Class E (Low side) inverter diagram

Anexa 4. Class E inverter (High side) PCB wiring

Anexa 5. Class E inverter (Low side) PCB wiring